Design and Aeroelastic Analysis of Flexible Wind Turbine Blades

Highly flexible materials in wind turbine blades to reduce maximum loading without compromising energy yield

S. Reijniers

Delft University of Technology

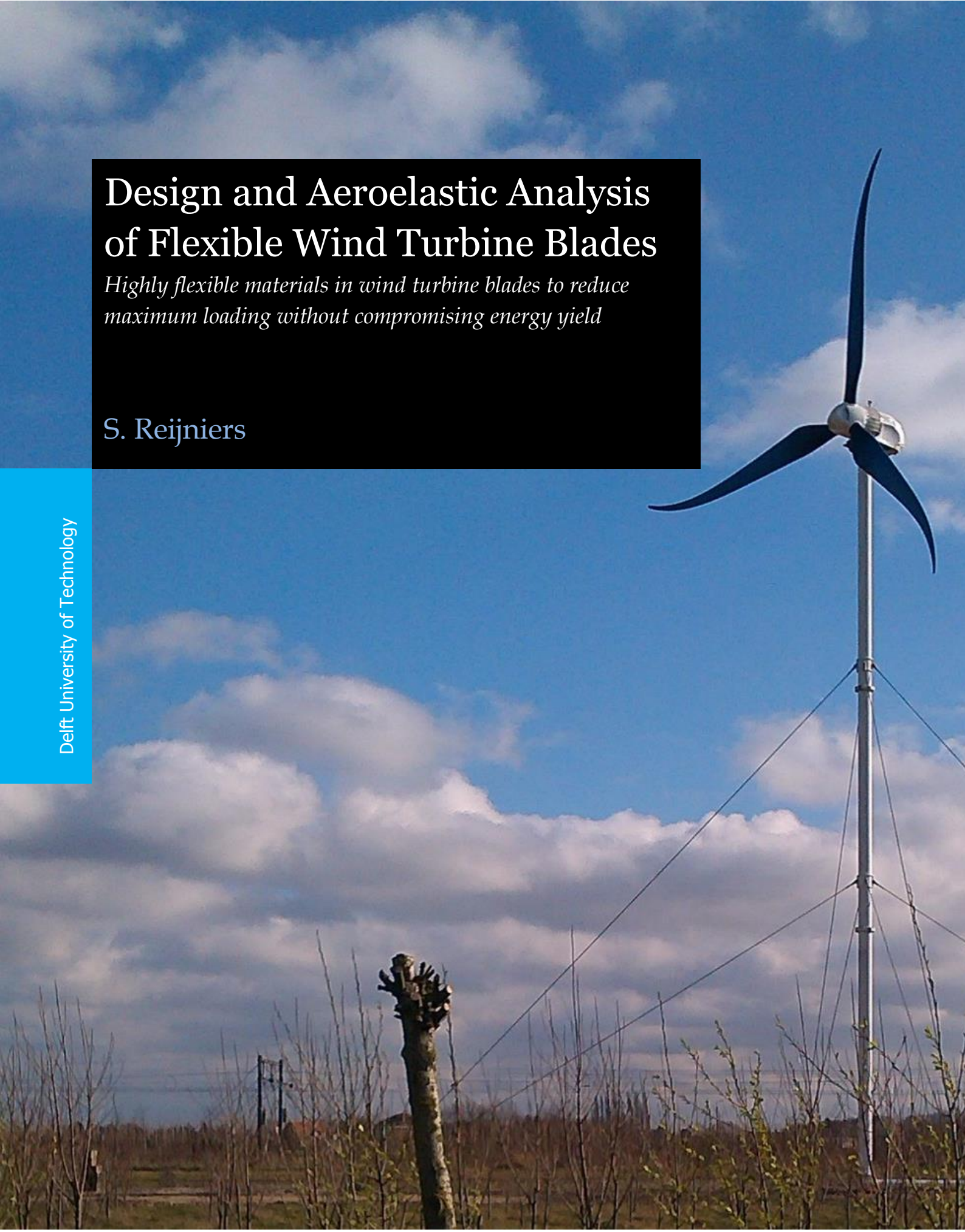

TU Delft Delft University of Technology

XANT

Challenge the future

Cover picture: XANT M-21 wind turbine, from www.windkracht13.be

Design and Aeroelastic Analysis of Flexible Wind Turbine Blades

For obtaining the degree
of Master of Science in Sustainable Energy Technology
at Delft University of Technology

The research has been carried out with the Wind Energy Research Group, Faculty of Aerospace Engineering, Delft University of Technology and with the company XANT

Simon Reijniers
July 2, 2015

This thesis is confidential and cannot be made public until July 2, 2020

Professor:	Prof. dr. G.J.W. van Bussel	TU Delft
Reader:	Prof.dr.ir. G.A.M. van Kuik	TU Delft
Supervisors:	dr. ir. Roeland De Breuker	TU Delft
	ir. Alex De Broe	XANT
	ir. Roland Broers	XANT

Summary

A wind turbine is designed to produce a maximum amount of energy at minimum cost while it withstands any possible wind condition. In the wind conditions with the highest wind speeds the wind turbine has to cope with the most extreme loads. In these most extreme cases the wind turbine is *parked*, the blades do not rotate, and the blades deform elastically under these wind loads. An increase in the flexibility of the blades results in higher elastic blade deformations. The main objective of this project is to design blades in a way that the extreme loading on the blades reduces with more than 10 % without compromising the energy yield by making use of flexible materials and the corresponding increased deformations. The reason to focus on load reduction is that a wind turbine can be made cheaper if these loads are reduced.

The research methodology is a three-step approach: Firstly a modelling tool is created to design and evaluate blades with new flexible materials at different locations in the blade. Secondly a verification procedure is performed to check the accuracy of the modelling tool. Thirdly this tool is used to design blades with highly flexible materials and to perform an iteration procedure to design the *best flexible blade design*.

The modelling tool is based on the cross sectional software BECAS to design new flexible blades and on the aeroelastic software HAWC2 to analyse the behaviour. This BECAS-HAWC2 modelling tool is based on the existing XANT M-21 wind turbine of which only the blade materials are variable parameters, the rest of the wind turbine remains as it is.

A verification procedure compares the modelling tool with two other models of the same blade. The minor differences between several modelled parameters increase the confidence in the BECAS-HAWC2 model.

A material with unidirectional fibres and a highly flexible matrix material is stacked in different orientations to design different blade materials. These flexible materials are introduced in specific locations of the blade. The design exploration approach makes it possible to design and evaluate many different blades using different flexible materials at different locations.

The current results show that the best option is to use the flexible material with fibres only in longitudinal and transverse direction in the skin of the blade. Not replacing the full skin but only the part of the root up to the middle of the blade results in the best flexible design. This best design has a reduction in maximum thrust force and maximum root bending moment of respectively 23 % and 26 % compared with the original blade, easily exceeding the predefined goal of 10 %. This significant load reduction is due to a significant blade twist rotation thereby reducing the area exposed to the wind. The annual energy yield is not compromised, it even shows a considerable 11 % increase due to a stall delay effect in the higher wind regimes which is also caused by an increase in blade twist.

The best flexible design is a preliminary design that shows promising results. These results show that by using flexible materials in the blade skin a significant load reduction is combined with an increase in energy. This indicates an untapped potential for future wind energy which makes further research on this topic recommended.

Acknowledgements

I would like to thank some people who helped me in the process of my thesis project.

At first thanks to my TU Delft supervisor Roeland de Breuker and XANT supervisors Alex de Broe and Roland Broers. Roeland for the guidance, wise counsel and support during the meetings. Alex for giving me the opportunity to perform my thesis research with XANT on the XANT M-21 wind turbine and for the very effective helpful meetings. Roland for the continuous help, support and pleasant times in Brussels. Thanks to Bram Lof, my enthusiastic thesis companion in Brussels who made thesis life less heavy. I had a nice time at the XANT offices in Brussels as well as in the Wind Energy Department of Delft University of Technology.

David Verelst has lots of relevant knowledge on my subject and was willing to help me in his free time. Special thanks since he is a real open-source-man while my thesis is confidential.

Except for the technical help there are many people who supported me in this long thesis process. Thanks to my girlfriend for the patience in the difficult times and to my family and friends for the support. Also thanks to the student advisor Leonie Boortman for the counsel in the most difficult times.

Table of Contents

List of figures iv
List of tables vii
Nomenclature viii
Abbreviations viii
Symbols viii
1 Introduction 1
1.1 Background 1
1.2 Problem definition 2
1.3 Report outline 3
2 Literature review 4
2.1 Bend-twist coupling 4
2.2 Load reduction 6
2.3 Passive power control 7
2.4 Blade instabilities 8
3 Modelling procedure 10
3.1 Base wind turbine 10
3.1.1 XANT M-21 10
3.1.2 Wind turbine blade layup 10
3.2 Aeroelastic modelling 11
3.2.1 Structural versus aerodynamic modelling 11
3.2.2 Simulation software tools 12
3.2.3 Choice for HAWC2 12
3.3 Modelling nonlinear versus linear material stiffness 13
3.4 Simulation procedure 14
3.4.1 Modelling setup 14
3.4.2 Design variables 14
3.5 Pre-processing 15
3.5.1 Input parameters 16
3.5.2 Software BECAS 16
3.5.3 Generation of the structural input file for HAWC2 17
3.5.4 Combination of cross sections 21
3.5.5 HAWC2 preparation 21
3.6 Processing: Main software component HAWC2 22

3.6.1 Structural model 22
3.6.2 Aerodynamic model 25
3.6.3 Wind model 25
3.6.4 Limitations of HAWC2 25
3.7 Post-processing 26
3.7.1 Preliminary stability analysis 26
3.7.2 Annual energy yield 27
3.7.3 Maximum loading 27
3.7.4 Limitations and assumptions 28
4 Verification of the tool 29
4.1 Models used in the verification 29
4.1.1 FOCUS6-HAWC2 model 29
4.1.2 ABAQUS-HAWC2aero model 30
4.2 Verification steps 30
4.2.1 Dynamic comparison 31
4.2.2 Response to static loading 35
4.2.3 Mass 38
4.2.4 Stiffness 40
4.2.5 Eigenfrequencies 42
4.3 Analysis of differences and similarities 43
4.3.1 Measurement data 43
4.3.2 Edgewise behaviour 43
4.3.3 Flapwise behaviour 44
4.3.4 Torsional behaviour 44
4.4 Summary 45
5 Blade design setup and results 46
5.1 New blade design 46
5.1.1 Effect of spar cap and skin material 46
5.1.2 Wind turbine blade materials 47
5.1.3 Selection of flexible 3D material properties 47
5.1.4 Change the skin with flexible 0-90 deg laminate 51
5.1.5 Change the skin with flexible +/-45 deg laminate 51
5.1.6 Change the complete spar cap with flexible unidirectional laminate 52
5.2 Key performance indicators 52
5.3 Results 52

Step I: Flexible material in full blade 53
Step II: Partial flexibility 1 53
Step III: Partial flexibility 2 55
Step IV: Partial flexibility 3 56
5.4 Summarizing analysis of best flexible design 57
5.4.1 Limitations 58
5.4.2 Increase in annual energy yield 58
5.4.3 Reduction in loading 60
6 Conclusions 62
7 Recommendations for future work 64
8 Bibliography 65
Appendix A Aeroelastic instabilities related to bend-twist coupling 68
Appendix B Section reduction 70
Appendix C Nonlinear modelling 72
Appendix D HAWC2 twist output 75
Appendix E Load reduction to cost relation 76
Appendix F Manual master thesis software tool 77
F.1 Required software 77
F.2 User's manual 77
F.2.1 Adapt the input Matrix 77
F.2.2 Prepare and perform the pre-processing 78
F.2.3 Prepare and perform the processing 79
F.2.4 Prepare and perform the post-processing 80

List of figures

Figure 1 – XANT M-21 wind turbine [1] 1

Figure 2 – Schematic representation of moments and displacements in the three principle blade directions: flapwise, edgewise and torsional [3] 4

Figure 3 – Bend–twist coupling due to off-axis fibres in the composite layup. (a) shows the axial layup and (b) the off-axis layup. [5] 5

Figure 4 – Bend–twist coupling due to swept blade planform. This is the bend-twist coupling present in the XANT M-21 wind turbine [6] 6

Figure 5 – The blade root flapwise bending moment of a swept blade (STAR6) and a blade without sweep (BASE6) are shown. This shows that by introducing sweep in the blade and therefore introducing a bend-twist coupling the operational blade loads can be reduced. This is done without compromising the energy yield. [6] 7

Figure 6 – Geometry and main material types of a cross section at 75 % of the blade 11

Figure 7 - Stress-strain response of a flexible material sample at different strain rates showing nonlinear stiffness and hysteresis behaviour [18] 13

Figure 8 - Basic modelling scheme of the modelling procedure of this research 14

Figure 9 – Pre-processing modelling scheme 15

Figure 10 – BECAS program modules [22] 17

Figure 11 – Input data and intermediate calculation tools to calculate the blade part of the structural HAWC2 file 17

Figure 12 – Sequence of nodes and key points in Airfoil2BECAS [23] 18

Figure 13 - Input files for Airfoil2BECAS 19

Figure 14 – Cross sections tilt: the black cross section line corresponds to the definition of the cross sections, the red cross section line shows how HAWC2 assumes the cross sectional properties are modelled, the green line is the approximate centreline 20

Figure 15 – Layup spar cap: BECAS format (a) and real ply stacking (b) 20

Figure 16 – Example of a combination procedure 21

Figure 17 – Multibody formulation in HAWC2 [28] 23

Figure 18 – Multibody formulation of the blade part of the XANT M-21 HAWC2-model 24

Figure 19 – Power curve and Weibull distribution 27

Figure 20 – Flapwise bending and centrifugal stiffening 32

Figure 21 – Dynamic comparison of power and thrust force and of the tip displacements and root bending moments in three directions (flapwise, edgewise and torsional). Results for the three different verification models are shown. 34

Figure 22 – Static flapwise and edgewise tip loading of 50 kg. The static response under these loads is compared for the BECAS-HAWC2 and the ABAQUS model. 35

Figure 23 - Edgewise displacement under edgewise static tip loading for BECAS-HAWC2 and ABAQUS model. Also the difference between the two models is shown. 36

Figure 24 – Flapwise blade displacement under flapwise static tip loading for BECAS-HAWC2 and ABAQUS model. Also the difference between the two models is shown. 37

Figure 25 – Blade twist under flapwise static tip loading for BECAS-HAWC2 and ABAQUS model. Also the difference between the two models is shown..... 38

Figure 26 – Absolute blade mass of BECAS, FOCUS6 and ABAQUS model and the difference of ABAQUS and FOCUS6 model w.r.t. BECAS model..... 39

Figure 27 – Distributed stiffness properties calculated with BECAS and FOCUS6..... 41

Figure 28 - Difference of the stiffness properties calculated with FOCUS6 w.r.t. the values of BECAS (see Figure 27)..... 41

Figure 29 – Schematic image of the unidirectional base ply and the principle ply directions [35] 48

Figure 30 – Design of the laminate from the base ply [37]..... 49

Figure 31 – Three different blade designs with flexible ply..... 50

Figure 32 - The structural and mass properties of three adapted blades: the skin is replaced with the flexible +/- 45 deg laminate (top right) or the 0 – 90 deg laminate (top left) or the full spar cap is replaced with the unidirectional ply (bottom). The values are normalised w.r.t. the original unchanged blade properties. 51

Figure 33 - The blade is divided in two, three, seven and 14 cross sections. One by one each of these cross sections is made flexible. The coloured sections indicate which skin sections should be changed with BD 0-90 deg material to reduce the load-of-energy with more than 5 %. 54

Figure 34 – Maximum thrust, maximum root bending moment and annual energy yield of blades partially made of +/- 45 deg and 0-90 deg flexible blade material..... 55

Figure 35 – The skin is replaced with flexible +/- 90 deg material. Only a part of the blade is made flexible..... 56

Figure 36 – Length variation of the flexible part with 0-90 deg flexible laminate in the skin..... 57

Figure 37 - Change in annual energy yield, maximum thrust force and the ratio between these two by varying flexible root length 57

Figure 38 – Power curve, original and flexible root (5m) and Weibull probability density distribution for 10 m/s average wind speed..... 59

Figure 39 – AEY for different wind speeds of the original blade and the best flexible design..... 59

Figure 40 – Tip twist of the original blade and the new flexible blade 60

Figure 41 - Blade twist over the length of the blade, stand still under 70 m/s steady wind speed..... 61

Figure 42 – Aeroelastic stability boundaries for a bend-twist coupled blade. This research focusses on increasing the twist-to-feather coupling of the blade. The figure shows that in this case the flutter behaviour gets more critical while divergence limits increase. [41] 69

Figure 43 - HAWC2 dynamic simulation in the operational wind speed range, simulation results of which the blade is composed of 6, 11 or 28 structural sections 71

Figure 44 – Modelling of nonlinear materials in wind turbine blades with BECAS and HAWC2: a setup 72

Figure 45 – Material stiffness update. 73

Figure 46 – Calculation of the blade twist: automatic HAWC2 method versus manual dummy method 75
Figure 47 – MatProps input matrix 78
Figure 48 - CombinationOverview.xlsx 79
Figure 49 – Excel Multimodel 1 80
Figure 50 – Excel Multimodel 2 80

List of tables

Table 1 - Differences between resonance and aeroelastic instabilities [13] 9
Table 2 – XANT M-21 wind turbine main characteristics 10
Table 3 – Material properties are the variables of the input matrix 16
Table 4 – 19 HAWC2 structural parameters [25] 24
Table 5 – Simulation models included in this verification procedure 29
Table 6 - Verification parameters for the different models. Green indicates the data is included in the verification while red indicates it is not. 31
Table 7 – Root moments under tip loading of 50 kg for the ABAQUS and BECAS-HAWC2 mode .. 36
Table 8 – Total mass of structural blade models and 39
Table 9 - Location of the centre of gravity 40
Table 10 - Eigenfrequencies of the XANT M-21 wind turbine 43
Table 11 – Change in stiffness and mass properties when considering no spar cap or no skin 46
Table 12 - Stiffness parameters for unidirectional base ply 48
Table 13 – Stiffness parameters for ply and lamina 50
Table 14 – Key parameters for evaluations including parameter abbreviation and the desired trend... 52
Table 15 – Simulation steps to find best flexible design. Red shows negative results, green shows positive results. 53
Table 16 – Main energy and loading parameters from original and new flexible blade 57
Table 17 – Tip twist under extreme loading 60

Nomenclature

Abbreviations

AEY	Annual Energy Yield
BD	Bidirectional
BEM	Blade Element Momentum
DV	Design Variable
$\mathbf{F}_{T,max}$	Maximum Thrust Force
$\mathbf{M}_{root,max}$	Maximum Root Bending Moment
UD	Unidirectional

Symbols

a	Scale Parameter
k	Shape Parameter
m	Mass
E	Young's Modulus of Elasticity
$\mathbf{EI}_x$	Flapwise Bending Stiffness
$\mathbf{EI}_y$	Edgewise Bending Stiffness
G	Shear Modulus of Elasticity
GJ	Torsional Stiffness
$\mathbf{I}_x$	Flapwise Area Moment of Inertia
$\mathbf{I}_y$	Edgewise Area Moment of Inertia
J	Torsional Stiffness Constant
K	Stiffness
U	Wind Speed
ρ	Density
ν	Poisson Coefficient
$\boldsymbol{\omega}_n$	Eigenfrequency

1 Introduction

1.1 Background

Wind energy has a growing contribution to the energy mix. Mid-size wind turbines represent an untapped potential in industrialized and developing countries. The main challenge is to bring the cost-of-energy down of these wind turbines to make them economically interesting. This research focusses on the XANT M-21 wind turbine, a stall controlled mid-sized wind turbine (Figure 1).

Figure 1 – XANT M-21 wind turbine [1]

A wind turbine has long blades which are loaded by the wind. This wind loading is converted to electrical power output while the blades should be strong enough to withstand these wind loads. These loads on the blades are transferred to the tower, foundation etc. All components of the wind turbine are designed as such that they can deal with these loads without being damaged. One of the most extreme wind loads for which a wind turbine should be designed is a storm with wind speeds of 70 m/s [2]. In the case of this storm the wind turbine blades do not rotate and the wind turbine is in parked condition. This is one of the major design load cases. If the wind turbine can withstand this load case it will be safe in all other load cases. Reducing the peak loads on the wind turbine blades in this extreme case while keeping the power production the same is favourable. By reducing the peak loads the many components of the wind turbine such as the blade hub, tower, foundation, etc. can be downsized and therefore the wind turbine can be made cheaper. When the energy is kept the same while the loads and therefore the cost is reduced, the overall cost-of-energy will go down.

These extreme loads can be reduced in different ways. Pitch-controlled wind turbines can actively twist their blades to reduce the surface exposed to the wind. Stall-controlled wind turbines don't have such a pitch mechanism. "Aeroelastic tailoring" techniques can be used to reduce these peak loads without using active systems: blades deform elastically under the aerodynamic forces thereby reducing the surface exposed to the wind. This reduction in exposed surface reduces the blade loading. To obtain significant reduction in peak loading high deformations should be achieved.

The structural blade properties should be changed to achieve these high deformations. The search for non-conventional highly-flexible materials is essential as the current state-of-the-art glass fibre reinforced polymer blade materials are too rigid.

When cross-sectional structural properties are changed by using non-conventional highly–flexible materials in the blades, the behaviour of the wind turbine blade changes completely. This master thesis project addresses the design and analysis of a blade made of macro-elastic materials.

1.2 Problem definition

The following ***research question*** is formulated:

How should the different materials in the layup of a swept wind turbine blade be designed by making use of flexible materials in a way that the maximum loading decreases without compromising the energy yield?

The ***main objective*** is to design blades with highly flexible materials and to perform an analysis of these new blade designs to finally come to a blade design which reduces the extreme loading significantly without compromising the power output.

The ***research methodology*** is a three-step approach:

- Firstly a modelling tool is created to design blades with new flexible materials at different locations in the blade and evaluate these new blade designs
- Secondly a verification procedure is performed to check the accuracy of the modelling tool.
- Thirdly this tool is used to design blades with highly flexible materials and to perform an analysis of these new blade designs. An iteration procedure results in the *best flexible blade design*.

The XANT M-21 HAWC2 wind turbine model is used. Only the internal structural blade properties are changed while the rest of the wind turbine remains unchanged.

A combination of the software tools BECAS, HAWC2, and MATLAB is chosen to analyse the dynamic behaviour of different structural designs of the wind turbine blade.

1.3 Report outline

A literature review is presented in Chapter 2 where the effect of an increase in the bend-twist coupling of a wind turbine blade is described. Chapter 3 addresses the modelling tool which is made to design many flexible blades and evaluate these to find the blade with the highest load reduction and energy yield. To check if the modelling tool generates correct results a verification procedure is performed which is described in Chapter 4. In Chapter 5 this modelling tool is used and an iterative design approach is performed to finally come to the best flexible design. Finally the conclusions are presented in Chapter 6 followed by the recommendations in Chapter 7 which present the next steps to continue with this research.

2 Literature review

Under the aerodynamic loading the main deformation of conventional blades is a flapwise bending displacement. Due to the swept planform of the blade (see Figure 1) a twisting moment occurs which makes the blade twist around the longitudinal axis. This flapwise bending and induced twisting of the blade is called a *bend-twist coupling*.

The aim of this research is to reduce the extreme loading on the wind turbine while optimizing the power output by increasing the flexibility of the blade. Reducing the torsional stiffness of the blade increases the torsional deformation under the same loading conditions. The bend-twist coupling of the blade will therefore increase.

2.1 Bend-twist coupling

Figure 2 shows the main directions of the blade moments and corresponding displacement directions of a wind turbine blade which are flapwise, edgewise and torsional.

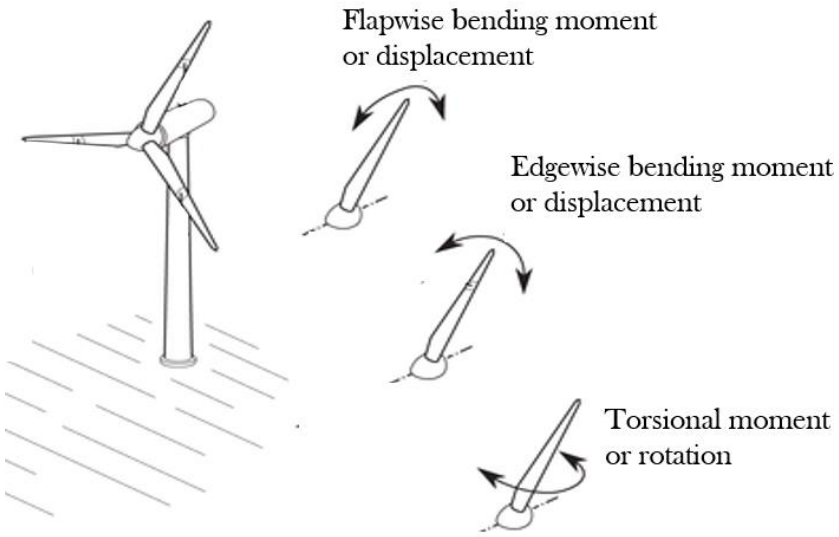

Figure 2 – Schematic representation of moments and displacements in the three principle blade directions: flapwise, edgewise and torsional [3]

A bend-twist coupling can be introduced in two ways:

- **Off-axis fibres in the composite layup:** The coupling is introduced by adapting the material of the blade. The fibre orientations are adapted to obtain a bend-twist coupling under blade loading (see Figure 3). The stress in the blade laminates tends to follow the fibre direction. Since these fibres are not oriented in the lengthwise direction, a shear stress component is induced and a torsional deformation occurs when the blade is under bending loads [4].

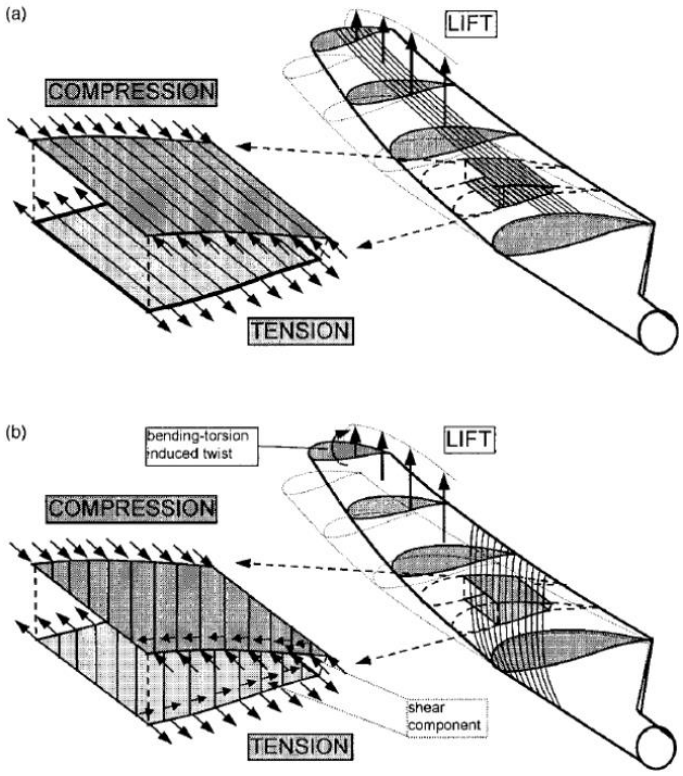

Figure 3 – Bend–twist coupling due to off-axis fibres in the composite layup. (a) shows the axial layup and (b) the off-axis layup. [5]

- **Swept blade planform**: The coupling is introduced by adapting the geometry of the blade (see Figure 4). The tip of the blade is moved backwards in the plane of rotation resulting in a *swept blade planform* as can be seen in Figure 4. When the blade tip is loaded this results in a moment over the blade resulting in a blade twist. A blade which is swept backwards against the rotational direction twists the blade thereby decreases the angle of attack in operation under wind loading. This is called a *twist-to-feather* motion (see Figure 4) and the coupling is called a bend-twist to feather coupling. A blade which is swept forward has a bend-twist to stall coupling which induces a *twist-to-stall* motion, an increase of the angle of attack under wind loading [4]. The XANT M-21 blade has a swept backwards blade planform.

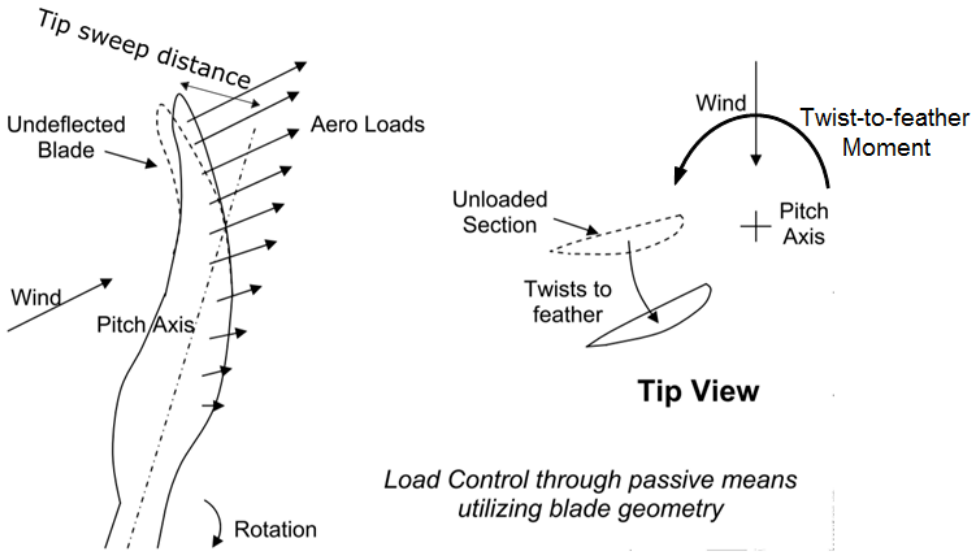

Figure 4 – Bend–twist coupling due to swept blade planform. This is the bend-twist coupling present in the XANT M-21 wind turbine [6]

The blade planform of the XANT M-21 wind turbine has a swept backwards planform with 1.2 m sweep at the tip (see Figure 4) of a blade of 10 m long. Therefore a twist-to-feather coupling is present in the blade.

The higher the torsional flexibility, the higher the bend-twist coupling of the blade. Several sources show that the loads on the wind turbine can be significantly reduced by increasing the bend-twist to feather coupling of the blade [6] [7] [8] [9].

2.2 Load reduction

A reduction in loading can be converted to a reduction in cost. It is also possible to translate it to an energy increase while maintaining the cost. The latter can be done by an elongation of the blades while maintaining blade loads below the original level. This blade elongation is further addressed in Appendix E. All mentioned increases of energy yield in this section are based on a load reduction and corresponding blade elongation.

In [8] a bend-twist coupling is designed in a wind turbine blade to induce a gain in annual energy yield up to 25 %.

In [6] a gain in energy yield of 5 – 10 % is found due to the bend-twist to feather coupling using sweep. Figure 5 shows the comparison between the long swept blade (STAR6) and a blade with the same length but without sweep (BASE6). This figure shows that the normalized bending loads of the swept back blade are reduced over the operating range. The power production of these same simulations remains the same.

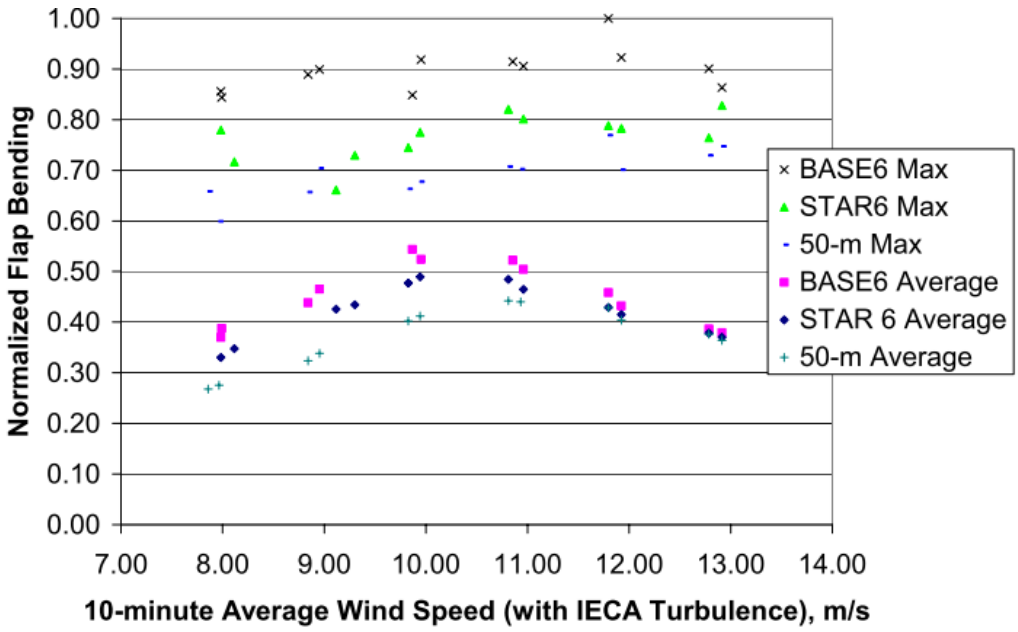

Figure 5 – The blade root flapwise bending moment of a swept blade (STAR6) and a blade without sweep (BASE6) are shown. This shows that by introducing sweep in the blade and therefore introducing a bend-twist coupling the operational blade loads can be reduced. This is done without compromising the energy yield. [6]

In [7] the focus lies on increasing the tip twist by reducing the torsional stiffness of a swept blade in a swept blade planform. A reduction in thickness of the airfoil is used to further reduce the torsional stiffness. As a result twist increases and reduces bending moments and fatigue.

Increasing a bend-twist to feather coupling may reduce the annual energy yield. If the initial twist distribution, minimum pitch angle and the balance of the elastic twist during operation are adapted to the desired shape and pitch angle the energy yield can be restored completely [9] [10].

[9] performs aeroelastic simulations with ADAMS including fatigue damage calculations. Simulations show a significant fatigue damage reduction of 20 – 80 % because of the implementation of a bend-twist coupling.

Concluding, the bend-twist to feather coupling can result in a load reduction without an energy decrease.

2.3 Passive power control

[11] performs numerical simulations to investigate the possibility to achieve passive control of constant power output with bend-twist coupled blades. This means having constant power over the rated operating range. The bend-twist to feather coupling is introduced by the fibre angles not by the sweep of the blade. To have this constant power output a tip twist of about 30 to 40 deg is required. To obtain the bending which results in the twist angle, high bending deflections are needed as well. The blades should be as lightweight as possible to minimise the restoring effect of the centrifugal loads.

The maximum levels of axial strain will be far greater than the typical values used in the design and they are likely to exceed the elastic limit.

An internship assignment has been performed prior to this thesis research by the same author of this thesis [12]. The effects of a stiffness reduction are analysed with HAWC2. The maximum thrust divided by annual energy yield is calculated as an indication of the cost-of-energy. No real material parameters are taken into account, the stiffness is generically changed to look for trends. The effect of an overall reduction in torsional as well as bending stiffness of a swept blade is analysed. While the annual energy yield is nearly constant, a significant reduction in maximum thrust force is found and therefore a reduction in cost-of-energy is concluded. A reduction of the torsional stiffness resulted in a significant "stall delay" effect, an increased energy production in higher wind regimes. The blade which is flexible in torsion remains near the maximum power while the original blade stalls at these high wind speeds. This is due to the twist-to-feather motion which reduces the angle of attack at these high wind speeds.

Concluding, passive power control in the rated operating range can be achieved by increasing the bend-twist to feather coupling.

2.4 Blade instabilities

The blade flexibility affects the stability. Instabilities may result in unwanted vibrations which in turn may cause structural failure. Since only the blade of the wind turbine is redesigned in this research, the focus lies on the instabilities related to the blade specifically. The main instabilities in the blade are resonance and aeroelastic instabilities. Increasing the flexibility of a wind turbine may result in resonance or aeroelastic stability issues. Some main differences between resonance and aeroelastic instabilities are shown in Table 1.

Resonance: Resonance occurs when an external excitation acts on the blade which is of the same frequency as one of its natural frequencies. If the system is excited at its eigenfrequency and there is not enough damping the amplitude of the vibration will increase in a linear manner. To avoid resonance, one has to know the eigenfrequencies accurately [13].

Aeroelastic instabilities: The field of aero-elasticity considers phenomena in which interactions occur between aerodynamic flows and elastic structures [14]. In a slender structure as a wind turbine blade which has low structural stiffness these interactions are significant. More explanation about the main aeroelastic instabilities as well as the effect of these instabilities of an increased bend-twist to feather coupling is shown in Appendix A.

Table 1 - Differences between resonance and aeroelastic instabilities [13]

Resonance	**Aeroelastic instabilities**
Dependent on frequency coincidence between forces and eigenfrequenies	Not dependent on frequency coincidence
Zero damping	Negative damping
Linear increasing vibrational amplitude	Exponential increasing vibrational amplitude

3 Modelling procedure

The main objective of this research is to design blades with highly flexible materials and to perform an analysis of these new blade designs. This chapter describes the simulation tool to design and evaluate these flexible blades.

3.1 Base wind turbine

This section describes the XANT M-21 wind turbine model which is used as base model in this simulation tool. Some basic parameters of the XANT M-21 wind turbine are presented as well as the structural blade layup.

3.1.1 XANT M-21

The base wind turbine which is redesigned is the XANT M-21, designed and build by XANT and can be seen in Figure 1. The wind turbine main characteristics are shown in Table 2.

Table 2 – XANT M-21 wind turbine main characteristics

Rating	100 kW
Rotor orientation, configuration	Downwind, 3 blades
Blade coning angle	10 deg
Control	Variable torque, Stall
Drivetrain	Direct drive
Rotor diameter	21 m
Cut in, rated, cut out wind speed	3m/s, 11 m/s, 20 m/s
Blade planform	Swept
Wind turbine class	Class Ia

A 100 kW rated wind turbine is considered to be mid-size. The average size of onshore turbines being manufactured today is around 2.5 – 3 MW with blades of about 50 m [15]. Domestic wind turbines of several hundreds of watts are considered small size wind turbines. XANT has chosen for a stall-controlled rotor to avoid the use of failure-prone pitch systems. Also the direct drive generator requires a minimum of fragile elements. The downwind configuration allows for design towards more flexible blades without a tower strike.

3.1.2 Wind turbine blade layup

This section provides an overview of the internal structure of the wind turbine blade (see Figure 6).

A wind turbine blade can be divided in two main parts:

- **Blade skins**: These form the aerodynamic shape and carry the torsional loads and a part of the bending loads.

- **Internal longitudinal spar caps and webs**: These carry the shear loads and the main part of the bending loads. They also restrain the cross section shape against deformation and the skin panels against buckling [16].

The materials used in the blade layup of the XANT M-21 wind turbine, as shown in Figure 6, are the following:

- The external panels are made from bidirectional (BD) glass fibre reinforced polymer material. The blade skin is in general symmetrical and therefore these external panels consist of an inner layer as well as an outer layer. The layup direction of the fibres is alternating between plus and minus 45 deg. Balsa wood is placed between the inner and outer layer to form a stiff sandwich structure to prevent buckling.
- The spar caps are made of unidirectional (UD) glass fibre reinforced polymer material with all fibres in the longitudinal direction.
- A single shear web is used which is made of PVC foam as core material and some bidirectional fibreglass layers on top.
- The spar cap layers are embedded in a continuous fibre mat layer to reduce impregnation time

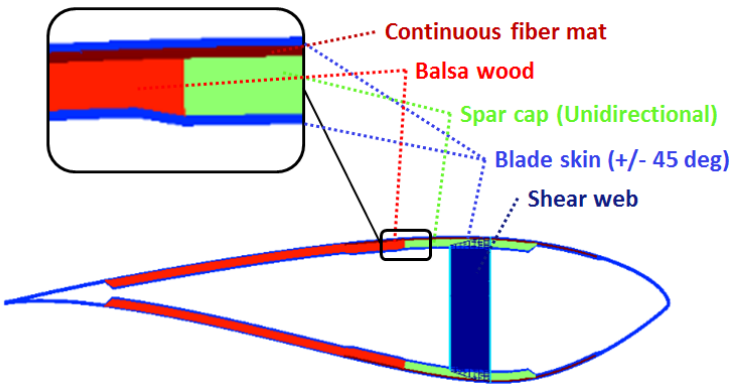

Figure 6 – Geometry and main material types of a cross section at 75 % of the blade

3.2 Aeroelastic modelling

This section describes some general aspects about aeroelastic modelling. The structural and aerodynamic modelling and their interactions are addressed. Simulation software modelling tools are described followed by the reasons to choose for HAWC2 as simulation software for the current modelling tool.

3.2.1 Structural versus aerodynamic modelling

A wind turbine blade deforms elastically under the aerodynamic loads and due to this elastic deformation the aerodynamics will change again. The amount of coupling between the structural

behaviour and aerodynamic effects defines if an approach with aeroelastic methods should be used or if the structural and aerodynamic behaviour can be analysed separately. In the case of a wind turbine blade this coupling is significant and therefore aeroelastic modelling tools are required. These structural and aerodynamic parts of the model are connected but solved separately and iteratively. These need to converge to a situation where they balance each other. Many different structural and aerodynamic software tools are available. The main difference is the level of complexity and the corresponding calculation time.

Aeroelastic simulation tools are used as a wind turbine design tool, to calculate performance, loads and displacements of the wind turbine in a predefined reference condition. A design tool should be able to perform multiple iterations in an efficient manner. Also the certification bodies require many load cases to be calculated increasing the required iterations. These stress the importance of short simulation times. On the contrary the convergence requirement between the structural and aerodynamic model of the coupled approach increases the simulation time very much w.r.t. using a structural and aerodynamic model separately. To keep short simulation times simplified aerodynamic and structural models are required.

3.2.2 Simulation software tools

Aeroelastic simulation design software comprises more than only aerodynamic and structural modelling. The main modelling parts which are all connected to each other in every aeroelastic design code are the following:

- Wind model
- Aerodynamic model
- Structural model
- Control model

In the context of a benchmark exercise (*Offshore Code Collaboration Exercise*, [17]) state of the art wind turbine simulation codes are evaluated against experimental data. Five major aeroelastic design codes are compared. The aerodynamic model of all these 5 design codes is based on the blade element momentum theory which is often improved with some correction models. All structural models are based on a multibody formulation or modal analysis. These are all reduced aerodynamic and structural models which are not computational expensive.

3.2.3 Choice for HAWC2

HAWC2 is used as the design tool for the modelling tool for different reasons:

- HAWC2 is the aeroelastic design software tool used to model the XANT M-21. The full HAWC2 model is available for this research.

- HAWC2 is a validated design code.
- Currently the main extra requirement is to have a tool which is able to accurately model a blade with high flexibility. A structural multibody formulation is a structural formulation which accounts for this flexibility and can still perform all the dynamic stimulations. HAWC2 is based on a multibody formulation.

3.3 Modelling nonlinear versus linear material stiffness

The stiffness of a material defines how a certain material deforms under a certain loading, it is the tangent of the stress-strain curve. When this stress strain curve is not a linear curve, the stiffness is not constant which indicates that different stiffness values should be used in the modelling. The stiffness is in this case dependent on the loading of the blade. Especially in the case of flexible materials this stiffness can change significantly. Another issue is the hysteresis effect where a retardation of the strain effect due to the stress in the material occurs. This way the stiffness is dependent on the past states. An example of a stress-strain curve of a type of a flexible material can be seen in Figure 7, which shows an example of a nonlinear stress-strain curve as well as the hysteresis effect.

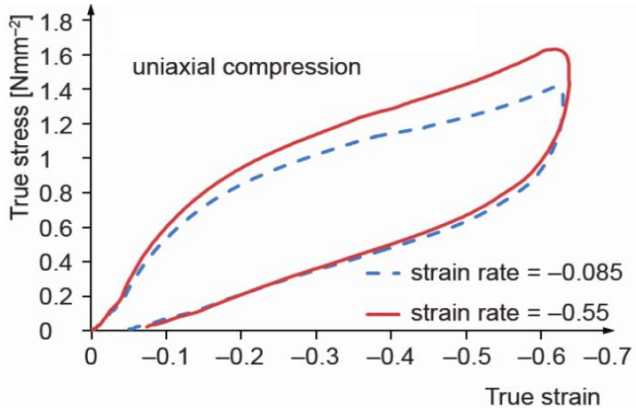

Figure 7 - Stress-strain response of a flexible material sample at different strain rates showing nonlinear stiffness and hysteresis behaviour [18]

Conventional aeroelastic simulation design programs assume linear material properties. Since conventional glass-fibre reinforced polymer material behaves very linearly this assumption is considered valid. Since flexible materials are used in this research, ignoring this nonlinear material behaviour could introduce significant errors. The original simulation setup includes material nonlinearities. Some major challenges to implement a nonlinear material model are however found:

- At least one extra iteration loop is needed which increases the complexity.
- Only steady simulations could be performed.
- Updating the stiffness properties is not convenient.

Therefore the modelling of nonlinear materials is considered to be out of the scope of this thesis. Therefore the assumption is made that every material has constant stiffness properties. Problems and possible solutions for the modelling of nonlinear materials are further explained in Appendix C.

3.4 Simulation procedure

This section describes the general setup which is used to model and analyse blades made of flexible materials. It is a limited overall description of the simulation setup which is further described in the following sections.

3.4.1 Modelling setup

The purpose of the modelling setup is to design blades with new blade materials at specific locations of the blade and to evaluate these new blades regarding power performance, maximum loading and stability. A design exploration method is used: multiple different cases are generated and analysed to come up with the best design. Therefore a fast modelling setup is required. A basic version of the modelling scheme can be seen in Figure 8.

Pre-processing: A certain material in a certain location of the blade is changed and the blade layup with the new material is converted to input files for the aeroelastic HAWC2 simulations **(**see section 3.5).

Processing: Aeroelastic HAWC2 simulations are performed with this new blade to generate the loads, displacements, power performance etc **(**see section 3.6).

Post-processing: A post-processing tool is generated to analyse the data of the new blade generated by HAWC2. The post-processing tool analyses the stability of the blades and calculates the maximum loading and the annual energy yield to find the optimum blade which has the highest load reduction and still produces the most energy (see section 3.7).

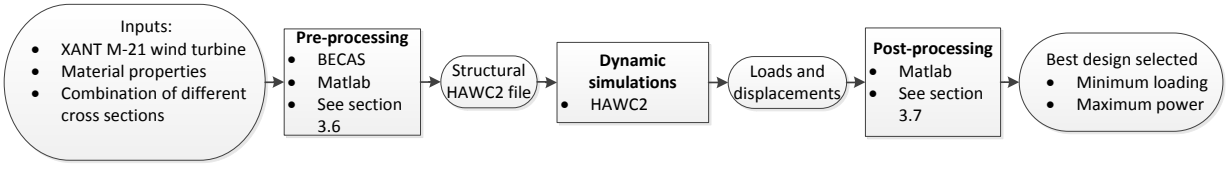

Figure 8 - Basic modelling scheme of the modelling procedure of this research

3.4.2 Design variables

To be able to investigate the effect of new blade materials but to keep the scope of the project feasible certain design variables (DV's) are identified. These are the main inputs for the pre-processing tool.

Only these design variables are changed, other parameters are kept the same as defined by the design of the XANT M-21 wind turbine. The design variables which have been selected are:

- **Type of material ply** (DV 1): Changing the type of the material means changing the material properties of a certain type of material. This means that the three-dimensional structural material properties of a certain blade part (see section 3.1.2) are adapted with flexible material properties.
- **Combination of different sections** (DV 2): With DV 1 cross sections are modelled over the whole blade which means 14 cross sections spread over the blade with the same DV 1. DV 2 is introduced by adding the option of combining cross sections with different DV 1. E.g. when a flexible and a rigid blade are designed with different DV 1's, DV 2 gives the opportunity to use the flexible blade cross sections in the root part and the rigid blade cross sections in the rest of the blade.

3.5 Pre-processing

The purpose of the pre-processing is to use the available inputs to prepare the necessary input files in the correct format to perform the dynamic simulations. Since many cases are considered this process is automated to make the process faster. A flow chart of the pre-processing modelling scheme can be seen in Figure 9.

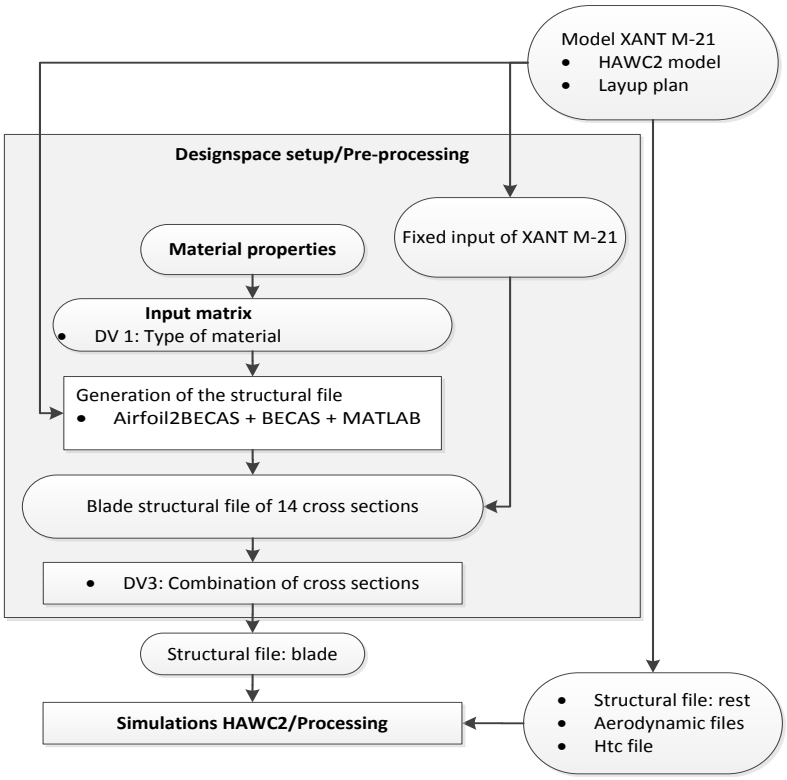

Figure 9 – Pre-processing modelling scheme

3.5.1 Input parameters

To generate a new blade an input matrix is made with the variable data which can be adapted easily. This input matrix comprises the material properties (design variable 1) for every type of material in the blade. These different blade material types are identified in section 3.1.2. The individual properties which can be changed are shown in Table 3.

Table 3 – Material properties are the variables of the input matrix

	Symbol	Definition
Design variable 1	E_1, E_2 and E_3	Young's modulus in three principle directions
	ν_{12}, ν_{13} and ν_{23}	Poisson coefficient in three principle directions
	G_{12}, G_{12} and G_{23}	Shear modulus in three principle directions
	ρ	Density

3.5.2 Software BECAS

BECAS is used to translate the detailed layup models to the structural properties for the HAWC2 model. This section describes the BECAS software in general.

BECAS is a software tool developed by the Danish Technical University. It is a MATLAB based finite element cross-sectional analysis tool used for section analysis of slender structures such as wind turbine blades. BECAS is an acronym for **BE**am **C**ross section **A**nalysis **S**oftware. It is developed at the same institute as HAWC2 and has a close relationship in the sense that structural outputs of BECAS can be used directly in HAWC2 which makes it a convenient tool to generate structural HAWC2 input. Only the pre-processing part of BECAS is used (see Figure 10). The post-processing part of BECAS can calculate the detailed three-dimensional stress and strain values due to the forces and moments resulting from the aeroelastic tool (HAWC2 in this case) which might be interesting for future research steps (see Chapter 7).

The structural input of 14 cross sections of the current HAWC2 beam model are developed. Such a cross section consists of different materials and a complex geometry summarized in 19 parameters. This is a complicated procedure for which different application tools are developed. BECAS is a finite element cross section analysis tool which determines structural properties of a beam cross section by calculating the complete cross section stiffness matrix. BECAS is based originally on the theory presented by Giavotto et al [19] and is implemented as a set of MATLAB functions by José P. Blasques [20]. The cross section analysis tool VABS is the state of the art in the field of cross section analysis tools and is used to validate the working of BECAS [21].

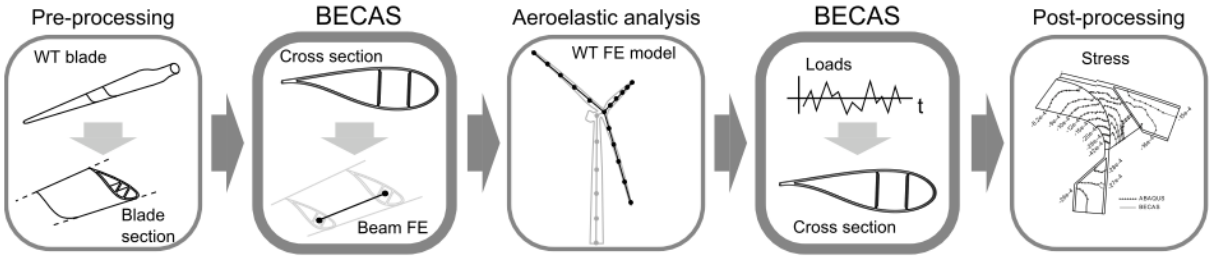

Figure 10 – BECAS program modules [22]

3.5.3 Generation of the structural input file for HAWC2

To go from the input matrix to the blade part of the structural HAWC2 input file an automated procedure is designed where Airfoil2BECAS and BECAS are coupled embedded in a MATLAB environment. This section addresses the use of BECAS in the current modelling tool.

BECAS pre-processing

BECAS is able to generate the structural HAWC2 input file from detailed layup information. Some extra steps are required to make this translation. An overview of the steps needed to come to the good input format for HAWC2 is shown in Figure 11.

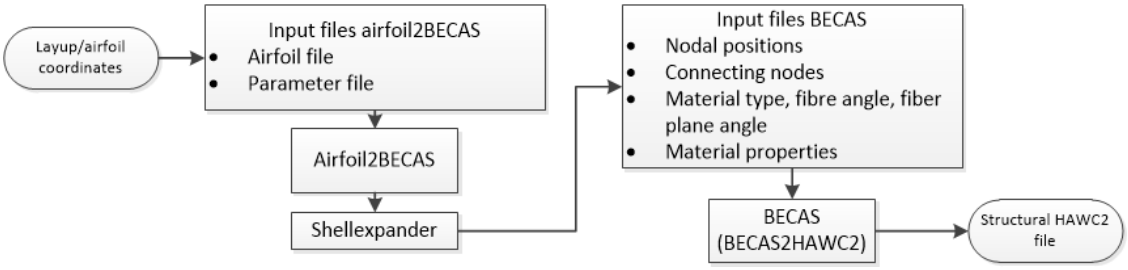

Figure 11 – Input data and intermediate calculation tools to calculate the blade part of the structural HAWC2 file

The BECAS input files contain:

- airfoil coordinates
- layup information
- material data

This information is contained in 4 input files:

1. N2D.in: List of nodal positions of the airfoil
2. E2D.in: List of connecting nodes
3. EMAT.in: List where material type, fibre angle and fibre plane angle are assigned
4. MATPROPS.in: List of material properties per material type

To generate these input files the python based software program **Shellexpander** is used. This program transfers cross sections in ABAQUS format to BECAS input files. Another python based program is available called **Airfoil2BECAS**. This prepares a "dummy" ABAQUS finite element shell model and calls shellexpander.py to process this file. Airfoil2BECAS generates a 2D-mesh of the cross section and the corresponding material orientation in BECAS format is generated.

The two input files for Airfoil2BECAS can be prepared from layup and airfoil coordinate data of wind turbine blades. The *first input file* is the airfoil file containing airfoil coordinates which are designed in a specific format and specific order according to Figure 12. From all the coordinates, nine key points are defined which divide the airfoil in eight regions, four upper and four lower regions. The *second input file* is the parameter file containing the rest of the blade data is combined:

- the exact layup of every region and every shear web with layer thickness, material type and layup orientation
- the amount of shear webs and their location
- the elastic properties in three directions of every material used

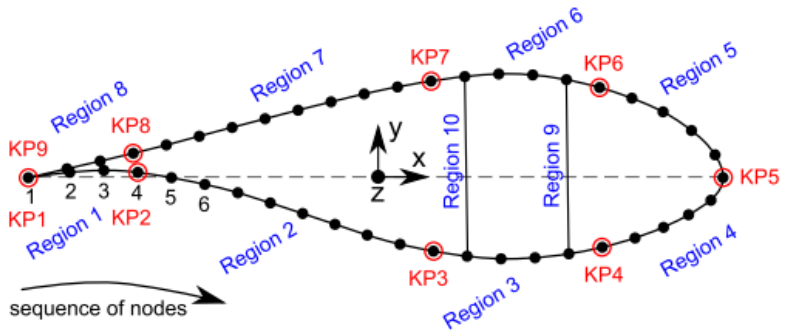

Figure 12 – Sequence of nodes and key points in Airfoil2BECAS [23]

An overview of the input files of Airfoil2BECAS and the input parameters used to generate these input files can be seen in Figure 13. The different steps to generate the BECAS model are the following:

- **Adapt Airfoil2BECAS**: The amount of discretisation nodes is increased to model cross sections in more detail.
- **Design the Airfoil file**: The airfoil file is defining the airfoil shape. It is a fixed input since this is not related to any variable input parameter. The design of the airfoil file is based on the airfoil coordinates of the XANT M-21 wind turbine. The 17 key points and the corresponding 16 regions are based on the layup scheme of the XANT M-21.
- **Design the parameter file**: The parameter file defines the thickness for every region separately and the material properties as well as the shear web location and design. This parameter file is not constant since the material thickness and material properties are the main

variable input parameters. In the automated loop the material properties and material thickness are updated with the parameters of the input matrix. By changing parameters of the input matrix the input files for Airfoil2BECAS can be updated as well using the MATLAB-embedded environment.

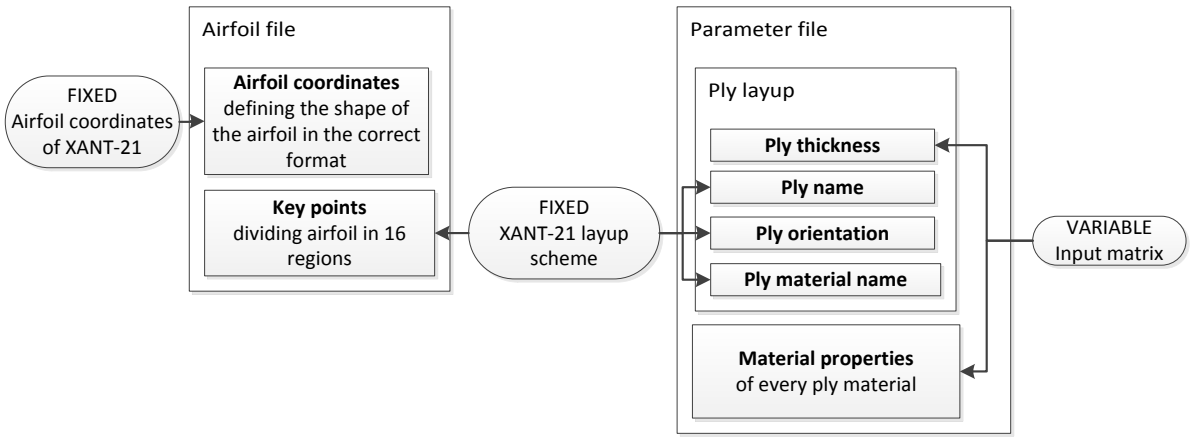

Figure 13 - Input files for Airfoil2BECAS

The design process to generate a cross section takes quite some time to perform accurately since it involves a significant amount of manual work. In the current modelling tool 14 cross sections are used, spread over the blade which is further addressed in Appendix B.

Some **extra modelling challenges** arise:

- **Fixed twist**: The shear web is not located vertically in every cross section. In the XANT M-21 blade the cross sections are individually twisted with respect to each other. The twist of the sections is applied explicitly in HAWC2. The shear web does not twist with the sections. In BECAS de sections are modelled with the chord of the section horizontally. To include the twist of the sections, the shear web is twisted with respect to the rest of the cross section depending on the structural twist angle.
- **Tilt:** The cross section properties in HAWC2 are dynamically modelled as if they are positioned perpendicular to the centreline of the blade. The cross section input properties used to design the BECAS cross sections assume the cross sections to be parallel to each other. Since the current blade has a swept planform, the centreline will be curved and the sections should always be perpendicular to this curved centreline. Therefore the coordinate file is tilted to account for the sweep as shown in Figure 14.

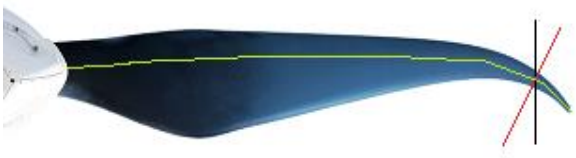

Figure 14 – Cross sections tilt: the black cross section line corresponds to the definition of the cross sections, the red cross section line shows how HAWC2 assumes the cross sectional properties are modelled, the green line is the approximate centreline

- The amount of regions of constant material properties and thickness used in Airfoil2BECAS is limited to 16. The most significant differences are located at locations with a sudden change in material thickness e.g. where the spar cap stops. There the program calculates a transition zone with a linear chamfer operation. While the spar cap in fact has a specific shape with a slope at the sides (see Figure 15 b), it is simulated in a more simplified manner as can be seen in Figure 15 a.

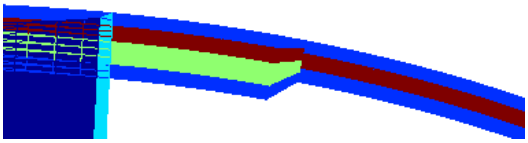

(a)

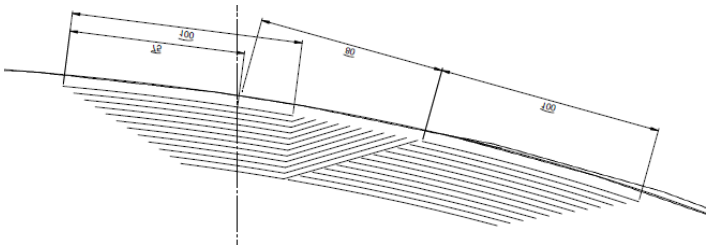

(b)

Figure 15 – Layup spar cap: BECAS format (a) and real ply stacking (b)

BECAS processing: structural file generation

Once Airfoil2BECAS is simulated, the input files for BECAS are ready and the BECAS simulations are performed. BECAS works in a MATLAB environment. Different modules are called one by one. Cross section properties are calculated and the structural set consisting of 19 HAWC2-parameters is generated (see Table 4).

3.5.4 Combination of cross sections

The blade part of the structural HAWC2 file contains 19 parameters for every one of the 14 cross sections. These 14 cross sections all have the same material laminates. To be able to change the structural properties not for the whole blade but for a certain lengthwise location only, different cross sections of different blades are mixed. An example of a combination procedure of two different blades can be seen in Figure 16.

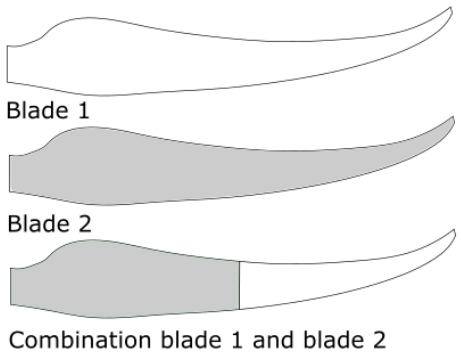

Figure 16 – Example of a combination procedure

3.5.5 HAWC2 preparation

For design certification hundreds of possible load cases are modelled in HAWC2 with varying wind speed and wind turbine setup. Since the purpose is to test many different cases in a fast way such a full design procedure is not relevant. Some determining load cases are selected to catch the general behaviour of the wind turbine:

1. steady uniform wind: power curve
2. Extreme Turbulence Model: maximum loading under operation
3. Extreme Wind Model: maximum loading in parked condition

Based on these load cases the wind turbine is evaluated regarding energy yield and maximum loading and stability.

Steady uniform wind: power curve

Steady uniform straight wind is used to calculate the power curve. The wind speed is stepwise increased from cut-in wind speed of 3 m/s up to the cut-out wind speed of 20 m/s in steps of 1 m/s. From this load case the power curve and the blade stability are extracted.

Maximum load in parked condition

When the wind speed increases to a certain level the wind turbine is “shut down”, this means the brakes are activated and the wind turbine stops rotating. This non-rotating wind turbine should resist a

maximum wind speed with a 50-year recurrence period according to IEC 61400 series standards. For a Class 1 wind turbine such as the XANT M-21 , considering steady wind this is a wind speed of 70m/s. This wind model is called the *Extreme Wind Model* [2]. The Blade Element Momentum (BEM) model (see section 3.6.2) which is used in HAWC2 is designed for an operating wind turbine and is based on induction, the retardation of the airflow over the homogeneous actuator disc. At standstill there is no induction and therefore the classical BEM code cannot be used anymore. This induction is switched off in HAWC2 and the model is changed to a basic blade element model. This blade element model divides the blade into discrete segments of which the aerodynamic forces and moments are calculated. These forces and moments are then summed to conclude the total forces [24].

Maximum load under operation

The maximum loading under operation is the Extreme Turbulence Model at the cut-out wind speed of 25 m/s. The maximum blade loading under operation is lower than the maximum loading in parked condition in all cases. Therefore to find the maximum load condition only the wind turbine in parked condition is considered.

3.6 Processing: Main software component HAWC2

This section addresses the processing part of the modelling tool: performing HAWC2simulations.

At the beginning of the design of the XANT M-21 HAWC2 was selected as the appropriate design tool. HAWC2 is an acronym for Horizontal Axis Wind turbine Code 2nd generation. It is an aeroelastic code developed by Risø – Danish Technical University. HAWC2 is a software tool used for the simulation of wind turbine response in the time domain for onshore, offshore and floating wind turbines. Since the focus will only be on the blade of the wind turbine the relevant program modules for this project are the structural, aerodynamic, and the wind module which are further described in sections 3.6.1 - 3.6.3. More details on how HAWC2 works can be found in the manual [25].

3.6.1 Structural model

The structural model consists of a multibody formulation where Timoshenko beam elements are coupled together as can be seen in Figure 17 and Figure 18. First the structural model is described in general, followed by the specific structural model used for this research.

Structural model in general

Every component or “main body” exists of one or more bodies each with their own reference frame. Every body is again separated in a set of Timoshenko beam elements. Each of these elements has constant stiffness, mass and inertia. BECAS is a suitable tool to generate these structural beam properties from layup data as is described in section 3.5.3.

A wind turbine blade is a three dimensional object. Even the full three-dimensional theory of elasticity is not perfect. Further assumptions to simplify the theory make the theory more widely applicable. Several one-dimensional beam theories have been developed based on various assumptions. The Timoshenko beam theory which is used in HAWC2 is similar to the Bernoulli-Euler beam theory model which is one of the most simple beam models developed in the 18th century. In 1921, Timoshenko improved this beam model by including shear. These models are further addressed in [26]. Inside each body linear formulation is used and therefore only small deflections are allowed. High deflections need to be modelled with multiple bodies. Also high blade twists are correctly modelled with HAWC2 [27]. Regarding the twist output there is no correct predefined tip twist in the root coordinate system available in HAWC2 which is further addressed in Appendix D.

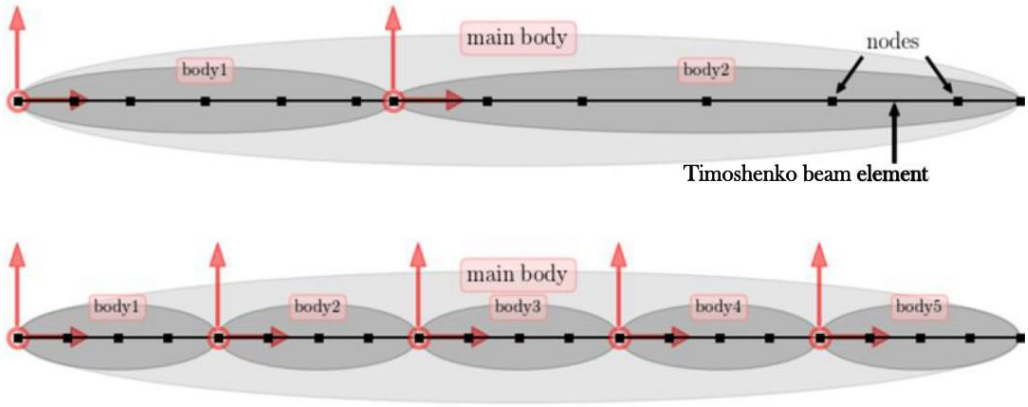

Figure 17 – Multibody formulation in HAWC2 [28]

An external structural input file contains 19 structural parameters per cross section of the as can be seen in Table 4. Only the structural behaviour is defined, the geometrical parameters which are the cause of this structural behaviour are all summarised in this set of one-dimensional structural beam properties. This file is changed to model new flexible blade designs.

Table 4 – 19 HAWC2 structural parameters [25]

Column	Parameter
1	r, curved length distance from main_body node 1 [m]
2	m, mass per unit length [kg/m]
3	x_m, x_{c2}-coordinate from $C_{1/2}$ to mass center [m]
4	y_m, y_{c2}-coordinate from $C_{1/2}$ to mass center [m]
5	r_{ix}, radius of gyration related to elastic center. Corresponds to rotation about principal bending x_e axis [m]
6	r_{iy}, radius of gyration related to elastic center. Corresponds to rotation about principal bending y_e axis [m]
7	x_s, x_{c2}-coordinate from $C_{1/2}$ to shear center [m]
8	y_s, y_{c2}-coordinate from $C_{1/2}$ to shear center [m]
9	E, modulus of elasticity [N/m^2]
10	G, shear modulus of elasticity [N/m^2]
11	I_x, area moment of inertia with respect to principal bending x_e axis [m^4]. This is the principal bending axis most parallel to the x_{c2} axis
12	I_y, area moment of inertia with respect to principal bending y_e axis [m^4]
13	K, torsional stiffness constant with respect to z_e axis at the shear center [m^4/rad]. For a circular section only this is identical to the polar moment of inertia.
14	k_x shear factor for force in principal bending x_e direction [-]
15	k_y, shear factor for force in principal bending y_e direction [-]
16	A, cross sectional area [m^2]
17	θ_s, structural pitch about z_{c2} axis. This is the angle between the x_{c2} -axis defined with the c2_def command and the main principal bending axis x_e.
18	x_e, x_{c2}-coordinate from $C_{1/2}$ to center of elasticity [m]
19	y_e, y_{c2}-coordinate from $C_{1/2}$ to center of elasticity [m]

Structural model used for this research

This section describes what the HAWC2 model of the blade of the XANT M-21 model looks like.

The blade of the XANT M-21 is modelled as one main body which is divided in 5 different bodies (see Figure 18). To model the blade 14 nodes and therefore 13 structural Timoshenko beam elements are used. More sections are needed at the root since the blade stiffness and mass properties are changing more rapidly in lengthwise direction.

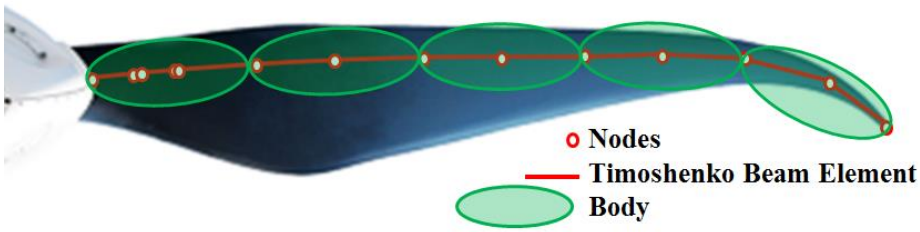

Figure 18 – Multibody formulation of the blade part of the XANT M-21 HAWC2-model

The research about the flexible blades will be conducted on the wind turbine blades only. Information about forces in the tower, foundations, hub etc. are not required. Some simplifications are therefore applied to the model of which the most significant is the replacement of tower with the guyed wires with an infinitely stiff standalone tower. This resulted in a significant reduction in simulation time. The guy wires are removed and the stiffness of the tower is increased up to practically infinite so no vibrational issues from the tower are taken into account, the focus lies therefore only on the blades.

3.6.2 Aerodynamic model

The aerodynamics module is based on Blade Element Momentum theory. BEM theory combines the local blade element theory and the global momentum theory to calculate the induced velocities. The main assumptions of these two theories are respectively [29]:

- The rotor acts as a frictionless, constantly loaded actuator disc therefore assuming an infinite number of blades.
- Each element is uniformly loaded, independent from the other elements.

HAWC2 contains some corrections on the classic BEM model [29]:

- non-uniform loading by calculating the induced velocities at every point of a discretized polar grid
- tip correction model: accounts for the finite number of blades
- skewed inflow model: accounts for variations in induced velocities
- dynamic inflow model: accounts for the transient in the rotor wake

3.6.3 Wind model

In the wind module deterministic wind parameters such as the shear, the gust, the tower shadow and stochastic parameters such as the build-in Mann turbulence generator and the dynamic wake meander model are included.

3.6.4 Limitations of HAWC2

Several major limitations of HAWC2 should be taken into account:

- **Material nonlinearity's:** One of the assumptions of the Timoshenko beam model in HAWC2 is that the material behaves linearly elastic. This is one of the major challenges which arises since flexible materials do not behave completely linearly and is therefore one of in the recommendations for future research in Chapter 7.
- **Timoshenko beam model:** The stiffness matrix in HAWC2 cannot model *internal* aeroelastic bend-twist couplings. In the stiffness matrix, which represents the linear relation between the forces and moments and the strains and curvatures, only the diagonal terms are present. The non-diagonal terms which model couplings between bending and torsion in a cross section are assumed to be zero. This simplification results in a much faster solving algorithm but a less accurate model if significant internal couplings between twist and bending deformations are present. These internal couplings are very significant when the bend-twist coupling is designed using directional material layers in a specific way (see section 2.1). If the coupling is introduced using a swept blade planform however, this coupling is an *external* bend-twist

coupling due to an externally generated moment which can be modelled correctly with HAWC2.

- **BEM:** HAWC2 is based on BEM theory which is based on several simplifying assumptions. Correction models are applied to adapt the wind turbine from ideal to real conditions but it is still a reduced aerodynamic model. E.g. when the blade is in operation under high deflections this changes the local induced velocities [30]. In the case of BEM the blade elements are independent, the model does not capture the influence that variations of aerodynamic loads at one radial position have on the loads at adjacent positions. These changes in induced velocities are therefore not calculated correctly [29].

3.7 Post-processing

This section describes how the HAWC2 simulation results are analysed. The blade is optimised by reducing the maximum loading while keeping or even increasing the energy production.

3.7.1 Preliminary stability analysis

To see if the new blade designs behave in a stable manner a simplified stability analysis is included in the modelling. Blade instabilities are addressed in section 2.4.

To check the stability of the wind turbine many load cases should be evaluated. For the purpose of this research the same case is used as for the power curve calculation (see section 3.5.5): steady uniform wind speed is stepwise increased from cut-in wind speed of 3 m/s up to the cut-out wind speed of 20 m/s in steps of 1 m/s. This case is considered to find the main instabilities. Since the wind turbine operates in the complete wind range and the steps trigger the major instabilities. An automated procedure is designed.

The divergent aeroelastic instabilities will make the simulation stop automatically if e.g. the deflections are too high for HAWC2 to cope with. Aeroelastic instabilities can however still be present in a converged load case, bringing major risks. Aeroelastic instabilities will first be seen at the tip since it is an unclamped end of the wing. The tip displacement amplitude is used as an indicator for instability. The current blade has a maximum tip displacement amplitude of 0.6 m. As long as this tip displacement amplitude of the new flexible cases is below 1 m it is considered to be stable.

The blade rotational velocity is another stability parameter which is monitored. Above the rated wind speed the torque controller keeps the rotational velocity constant. Changes to the torque controller design might however be required to cope with the new structural blade designs. This rotational stability parameter indicates if the torque controller without adaptations is good to use for the new blade design.

The control for aeroelastic instabilities does not point out which type of aeroelastic instability occurs. The HAWC2 simulations capture instabilities such as flutter and divergence (see section 2.4). However if e.g. a certain aeroelastic simulation is close to a certain instability but it is not triggered this cannot be seen. It will behave completely stable and no instabilities are found. A more elaborate stability research is recommended to map the major instabilities (see Chapter 7).

3.7.2 Annual energy yield

The power curve, calculated from uniform steady wind conditions (see section 3.5.5), is multiplied with a Weibull wind speed distribution to determine the annual energy yield. The Weibull equation is shown in equation 1 in which U is the wind speed, a is the scale parameter and k is the shape parameter [31]. Since it is a Class 1 wind turbine the average wind speed for which it is designed is 10 m/s which results in a Weibull scale parameter of 11.24 [31]. Assuming a wind field at the coast of the North-West of Europe a Weibull shape parameter of 2 is assumed [32]. The Weibull distribution is plotted together with the power curve of the XANT M-21 wind turbine in Figure 19.

$$f(U) = \frac{k}{a}\left(\frac{U}{a}\right)^{k-1} e^{-\left(\frac{U}{a}\right)^{k}} \qquad (1)$$

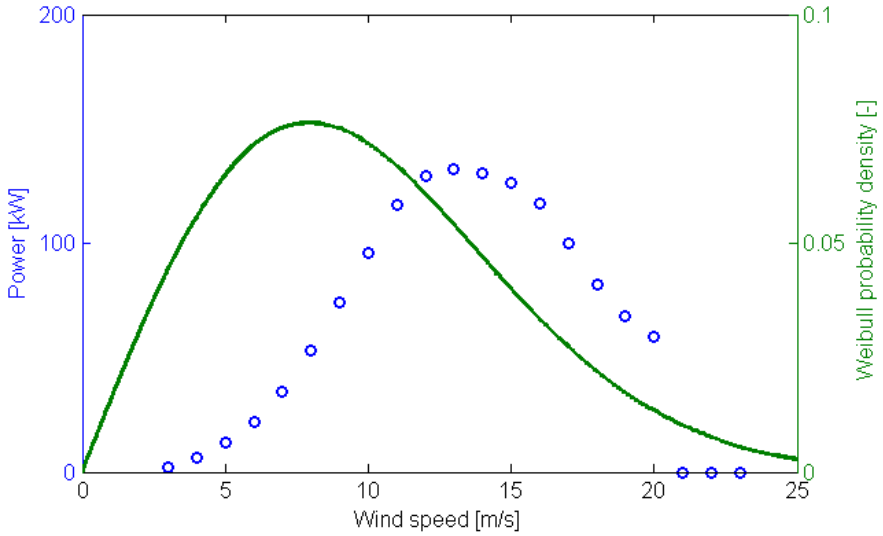

Figure 19 – Power curve and Weibull distribution

3.7.3 Maximum loading

The main design driving loads in a wind turbine are identified to be the following:

- maximum thrust force: affects mainly the tower and foundation sizing
- maximum flapwise root bending moment: affects mainly the hub sizing

The load case which is found to cause these maximum loads is the extreme wind model case with 70 m/s (see section 3.5.5).

3.7.4 Limitations and assumptions

Using this post-processing approach a judgement about a certain blade setup can be done which is based on the stability, the energy yield and two loads. This is an efficient way of calculating which option is best however several challenges are still present:

1. Parameters such as stability and maximum loading are calculated from the load case which is expected to be critical. This way the amount of load cases which is simulated for every case is limited. It could be that by using a certain flexible blade another load case is more critical. Since this research is based on relative results only, with the comparison with the original blade, it is not too important to be sure of the absolute maximum values.
2. The stress and strain in the material can exceed the maximum allowed stress and strain so the material would collapse (see recommendations in Chapter 7).
3. Buckling is not addressed yet (see recommendations in Chapter 7).
4. The current stability analysis is a preliminary stability check. A more elaborate stability analysis is required (see recommendations in Chapter 7).

4 Verification of the tool

This verification procedure focusses on the accuracy of the modelling tool described in Chapter 3. Full validation of the code with real measurement data would be best. Data about the total blade mass and eigenfrequency has been measured from the blade of the prototype and can be compared with the simulated data. The available validation data which can be compared exactly with the simulation data is however too limited to do a full validation analysis. A verification procedure in which the same blade of the XANT M-21 is modelled using different simulation tools is a more convenient way to investigate the accuracy of the results. This chapter describes a verification procedure, complemented with limited available validation data.

Only verification data of the original blade with conventional blade materials is available. Therefore the verification of the new flexible blade is considered out of the scope of the current research.

4.1 Models used in the verification

Except for the simulation modelling tool used for this research two other models of the same blade of the XANT M-21 are used in this verification procedure. Table 5 shows an overview of these three models indicating the aerodynamic and structural model as well as the model used to design the structural input properties for HAWC2/HAWC2aro.

Table 5 – Simulation models included in this verification procedure

	BECAS-HAWC2	FOCUS6-HAWC2	ABAQUS-HAWC2aero
Aerodynamic model	HAWC2	HAWC2	HAWC2aero
Structural properties	BECAS	FOCUS6	ABAQUS
Structural model	HAWC2	HAWC2	ABAQUS
Development	Current thesis research project	Blade developer	External party

4.1.1 FOCUS6-HAWC2 model

The FOCUS6-HAWC2 model is the original modelling setup which is used to design the current blade of the XANT M-21. The structural input file for the HAWC2 model is generated with FOCUS6. Some remarks:

- Very limited knowledge is available on how the structural model is designed and on which specific assumptions this is based.
- Only the structural input file is different from the BECAS-HAWC2 model, the aerodynamic and structural model are the same as these of the BECAS model. This allows to really focus on the structural file but cannot indicate limitations of the aerodynamic or structural model.

4.1.2 ABAQUS-HAWC2aero model

This model contains a structural shell-based finite element ABAQUS model of the blade which has been made in a project running parallel to this thesis research. This structural model is coupled with HAWC2aero, an aerodynamic simulation tool based on the aerodynamic model which is used in HAWC2. HAWC2aero is however not updated as often as HAWC2. Some remarks:

- The ABAQUS-HAWC2aero model has been built with the same modelling inputs as the BECAS model.
- This finite element shell ABAQUS model is more advanced than the Timoshenko beam model which is implemented in HAWC2. A Timoshenko beam model is a more simplified way of representing the structural properties of a wind turbine blade which makes the comparison with this more advanced shell model relevant. The structural ABAQUS model takes significantly more time to set up and perform simulations than the Timoshenko beam model. Therefore it is less useful to be used in iterative design.
- This ABAQUS-HAWC2aero coupling has not been extensively verified or validated as is HAWC2.

4.2 Verification steps

This section identifies the differences and similarities of the different blade models. These differences are analysed in the following section. A wind turbine design tool such as the BECAS-HAWC2 model has several main modelling parts which are coupled together. First the comparison of the dynamic results of the three models is performed. The differences in these dynamic results are further analysed by going more in detail about the different modelling blocks: the analysis of the static deflection, mass, stiffness and eigenfrequencies of the different models. The different parts of the tool which are verified can be seen in Table 6.

The main requirement to perform a verification is the availability of data which can be compared exactly. The simulation data of the two verification models is therefore limited to the availability of the data from the developers. In Table 6 the green blocks indicate which simulation part is taken into account in the verification while the red blocks indicate which parts are not.

Table 6 - Verification parameters for the different models. Green indicates the data is included in the verification while red indicates it is not.

Aeroelastic model	BECAS-HAWC2	FOCUS6-HAWC2	ABAQUS-HAWC2aero	Measurements on the prototype blade
Coupled model, semi dynamic				
Quasi-steady dynamic simulation output				
Structural model, static				
Response to simple static loading				
Eigenfrequencies				
Centre of gravity				
Stiffness distribution				
Mass distribution				
Total mass				

4.2.1 Dynamic comparison

This section compares the results of semi-dynamic simulations with the ABAQUS-HAWC2aero, BECAS-HAWC2 and FOCUS6-HAWC2 models. ABAQUS-HAWC2aero can only perform simulations in a steady-state environment without shear, gravity or tower shadow. To be able to compare apples with apples these steady-state conditions are applied to the HAWC2 simulations used in this comparison as well. The simulations are generated with the coupled tools where the structural and aerodynamic parts are combined.

The aeroelastic response of steady wind speed ranging from 3 to 18 m/s is shown in Figure 21. The ABAQUS outputs only starts from 7 m/s. Figure 2 in section 2.1 visualises the edgewise, flapwise and torsional moments and displacements of Figure 21.

Aerodynamic results

The power and rotor thrust force are shown in Figure 21 a and b respectively. These correspond well for all three models, no significant difference can be seen. Therefore it is concluded that the BECAS-HAWC2 model works well regarding power production and maximum thrust force.

Edgewise dynamic behaviour

The edgewise root bending moment and tip displacement are shown in Figure 21 c and d respectively. Comparison:

- The overall edgewise behaviour is similar for all three models.
- The BECAS-HAWC2 and FOCUS6-HAWC2 model have the same results.

- The ABAQUS-HAWC2aero model has a slightly higher moment than the other models. It also deviates regarding tip deflection. The tip deflection is lower, probably due to the higher root bending moment.

Flapwise dynamic behaviour

The flapwise root bending moment and tip displacement are shown in Figure 21 e and f respectively. The flapwise tip displacement without any wind loading is equal to zero. Once the wind turbine is in operation in a certain wind speed two main loads and corresponding deformations are present as is shown in Figure 20:

- The flapwise displacement under the aerodynamic loading is moving the blade with the wind.
- The flapwise displacement against the wind is due to the coning angle and corresponding centrifugal stiffening effect.

The centrifugal stiffening effect is the most significant below the rated wind speed which is 8 m/s with the current model. In this range a negative displacement value can be seen. This means that the blade tip is displaced more towards the wind than the original unloaded blade. Above the rated wind speed the rotational velocity remains the same as does therefore the centrifugal effect. The flapwise displacement under aerodynamic loading increases further which results in a positive tip displacement. Comparison:

- The overall behaviour is similar for all three models.
- The BECAS-HAWC2 and ABAQUS-HAWC2aero models behave the same.
- The FOCUS6-HAWC2 model has a higher root bending moment as well as a lower flapwise displacement.

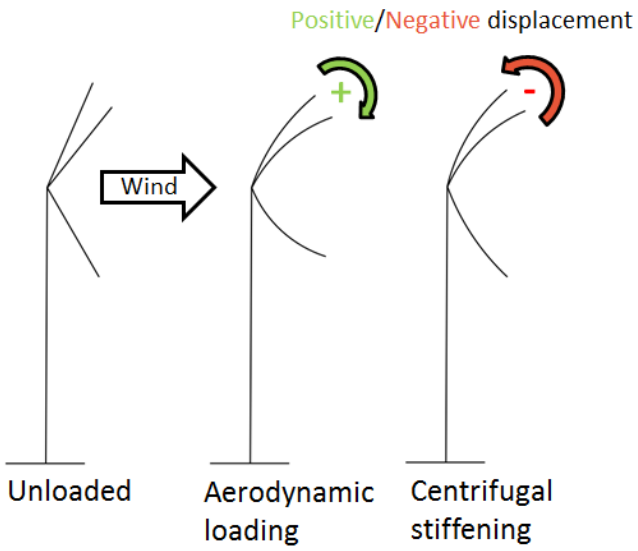

Figure 20 – Flapwise bending and centrifugal stiffening

Torsional dynamic behaviour

The torsional moment and tip twist are shown in Figure 21 g and h respectively. Comparison:

- A significant difference is present between the two HAWC2 models on one side and the ABAQUS-HAWC2aero model on the other side regarding the torsional root moment and the tip rotations. Under the same wind speeds ABAQUS-HAWC2aero shows higher tip rotations than the HAWC2 models. While the HAWC2 models do not go above 0.5 deg tip twist difference the ABAQUS-HAWC2aero model has tip twists up to 1.8 deg. There is not only an offset but also the general behaviour is different. It is however clear that tip twist and root twisting moment are closely related. Probably the difference in twisting moment causes this difference in tip twist rather than vice versa. The difference in tip twist up to about 1.9 deg is very unlikely to change the aerodynamics as much to cause such a significant change in the root bending moment. Therefore more research should be performed on how the twisting moment is calculated with these different tools which is considered out of the scope of this research.
- A difference is seen between the two HAWC2 models. The tip twist has a difference of about 30 % near the tip which is considered not too significant since this remains all below 0.5 deg while the ABAQUS models increases up to 1.8 deg tip twist.

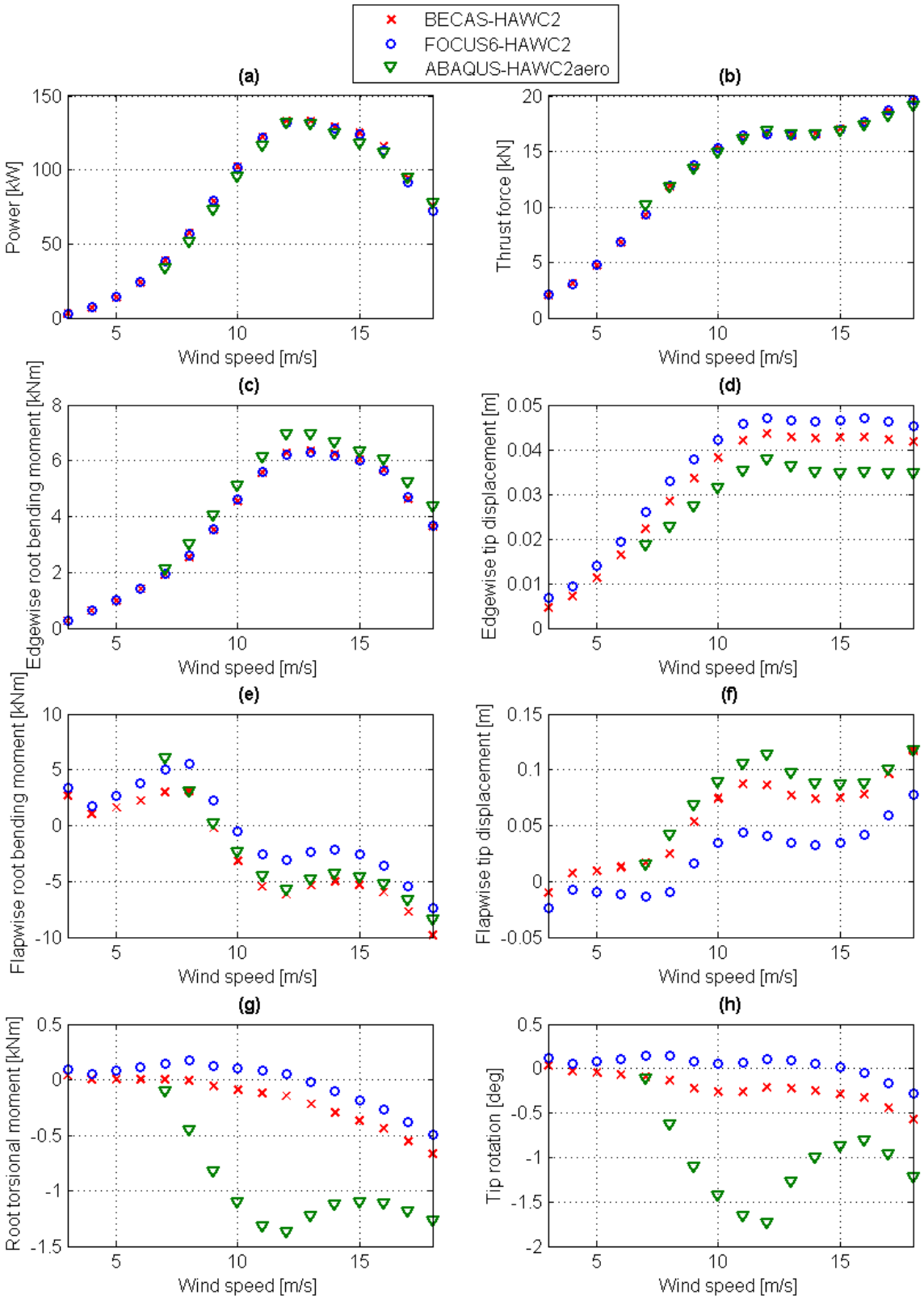

Figure 21 – Dynamic comparison of power and thrust force and of the tip displacements and root bending moments in three directions (flapwise, edgewise and torsional). Results for the three different verification models are shown.

4.2.2 Response to static loading

Differences are found in the previous section where aeroelastic simulation results are compared. To investigate what the cause is of these differences the structural models are compared separately from the aerodynamic models. This section addresses the behaviour of the structural model under static loading of 50 kg (490N) at the blade tip in flapwise and edgewise direction as is shown in Figure 22.

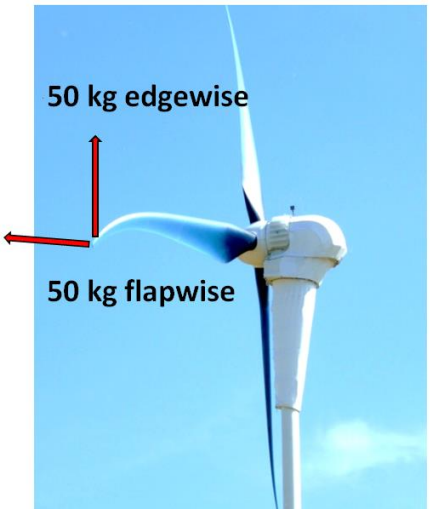

Figure 22 – Static flapwise and edgewise tip loading of 50 kg. The static response under these loads is compared for the BECAS-HAWC2 and the ABAQUS model.

The ABAQUS and BECAS-HAWC2 structural model are included in this comparison. To apply an external load on a HAWC2 model is not straightforward. Therefore the following steps are performed:

- The tip load is introduced as a tip mass of 490N while the mass of all other parts of the blade are made negligibly small.
- The blade is oriented in two different positions to extract the deflections of the load in flapwise and edgewise direction.
- No wind or other influences on the blade are taken into account except for the gravity and the tip mass, the rest of the wind turbine is massless.
- A HAWC2 simulation of 1000 seconds is performed in the time-domain to have all the motion damped out and find the static displacements, rotations and moments.

The root moments resulting from the tip load are compared for ABAQUS and BECAS in Table 7. All differences in moments are below 1 % so the BECAS-HAWC2 and ABAQUS static setup load introduction is considered the same. This confirms that when a load is introduced in the same way the correct moment is calculated.

Table 7 – Root moments under tip loading of 50 kg for the ABAQUS and BECAS-HAWC2 mode

Moments	Edgewise root bending moment [Nm]	Flapwise root bending moment [Nm]	Root torsional moment [Nm]
Loading	Edgewise	Flapwise	Flapwise
BECAS - HAWC2	4 896	4 899	584
ABAQUS	4 902	4 902	589
Difference [%]	0.12 %	0.06 %	0.88 %

Edgewise displacements

Figure 23 shows the blade displacement in edgewise direction of the BECAS-HAWC2 and ABAQUS model as well as the relative difference between the two models. Comparison:

- The edgewise curve fits well except near the tip where the ABAQUS blade seems to be more stiff than the BECAS blade.

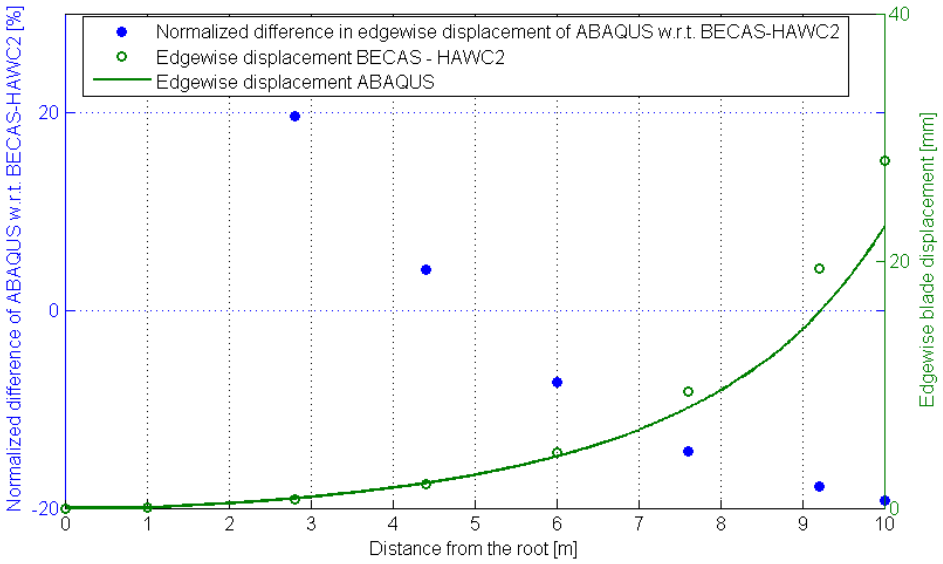

Figure 23 - Edgewise displacement under edgewise static tip loading for BECAS-HAWC2 and ABAQUS model. Also the difference between the two models is shown.

Flapwise displacements

Figure 24 shows the blade displacement in flapwise direction of the ABAQUS and BECAS-HAWC2 model as well as the relative difference between the two models. Comparison:

- Negligible differences up to only 5 % are present which confirms the results of the previous section: in flapwise direction the ABAQUS and BECAS-HAWC2 model are the same.

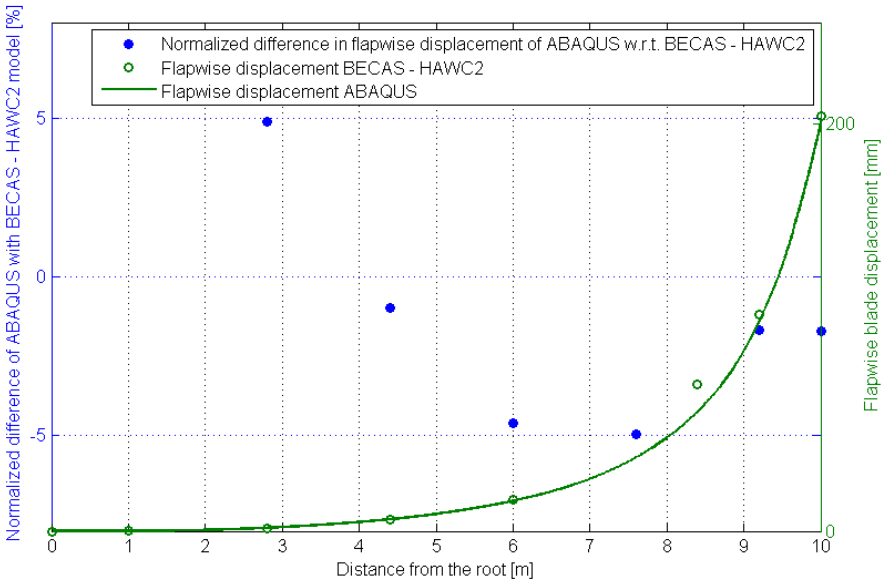

Figure 24 – Flapwise blade displacement under flapwise static tip loading for BECAS-HAWC2 and ABAQUS model. Also the difference between the two models is shown.

Twist

Figure 25 shows the blade twist of the ABAQUS and BECAS-HAWC2 model as well as the difference between the two models. In this case the applied moment is the same, which is not the case in the previous section where the semi-dynamic models are compared. Comparison:

- The largest absolute difference in blade twist can be seen near the tip. When the ABAQUS model is used the normalized difference shows that the twist of this tip part is up to 50 % higher than the rotations of the BECAS-HAWC2 model. The relative errors are increasing towards the root. This shows that the two structural models behave differently regarding blade rotations, also if the applied moment is the same. The differences are however multiple times smaller than the differences shown in the previous section where the dynamic models are compared.

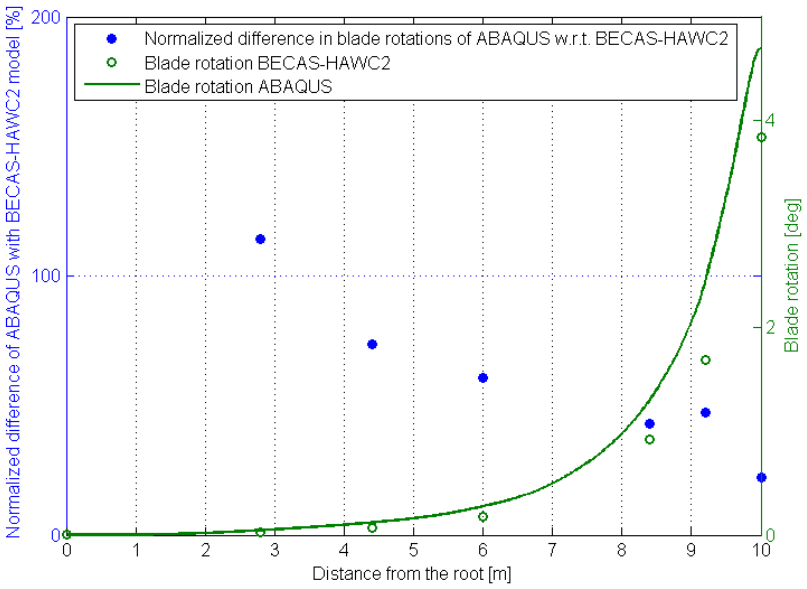

Figure 25 – Blade twist under flapwise static tip loading for BECAS-HAWC2 and ABAQUS model. Also the difference between the two models is shown.

4.2.3 Mass

Differences are identified between the three models in the previous sections. To further go into the detailed comparison of the structural model, the mass of the three models is compared in this section.

Total mass

The total mass of the blade is calculated with the three models. A measurement of the prototype total blade mass is available (see Table 8). Comparison:

- All modelled blade masses are within 6 % of each other and the BECAS model is the lightest of the models.
- The measured blade mass is 11 % higher than this of the BECAS-HAWC2 model. There are several reasons why this could deviate. The real material densities or the amount of material in the blades might be different from the modelling values. The focus is not on the absolute validation but rather on the verification between the models. This verification is included to see if the simulation models behave the same with the same design input data (material density, blade layup, etc.) rather than to check if the design input data itself is correct. Therefore this mass difference is not further taken into account.

Table 8 – Total mass of structural blade models and

Structural model	BECAS	FOCUS6	ABAQUS	Measurement
Mass [kg]	240	250	255	267
Difference with BECAS [%]		+4 %	+6 %	+11 %

Distributed mass

In Figure 26 the distributed mass over the blade can be seen for the three different models as well as the difference with the BECAS model. Comparison:

- All three distributions are very similar.
- Overall both the FOCUS6-HAWC2 and ABAQUS model seem to be slightly heavier than the BECAS-HAWC2 model.
- When zooming in on the outer 60 % of the blade, where the mass has more effect on the main behaviour, the ABAQUS model is on average lighter than the FOCUS6 model which is opposite to the total mass results of Table 8. In the ABAQUS model more mass is located near the root. This is confirmed by the comparison of the centre of gravity of the different models. Table 9 shows that the centre of gravity of the ABAQUS model is located more towards the root compared with the other models and the real measurement.

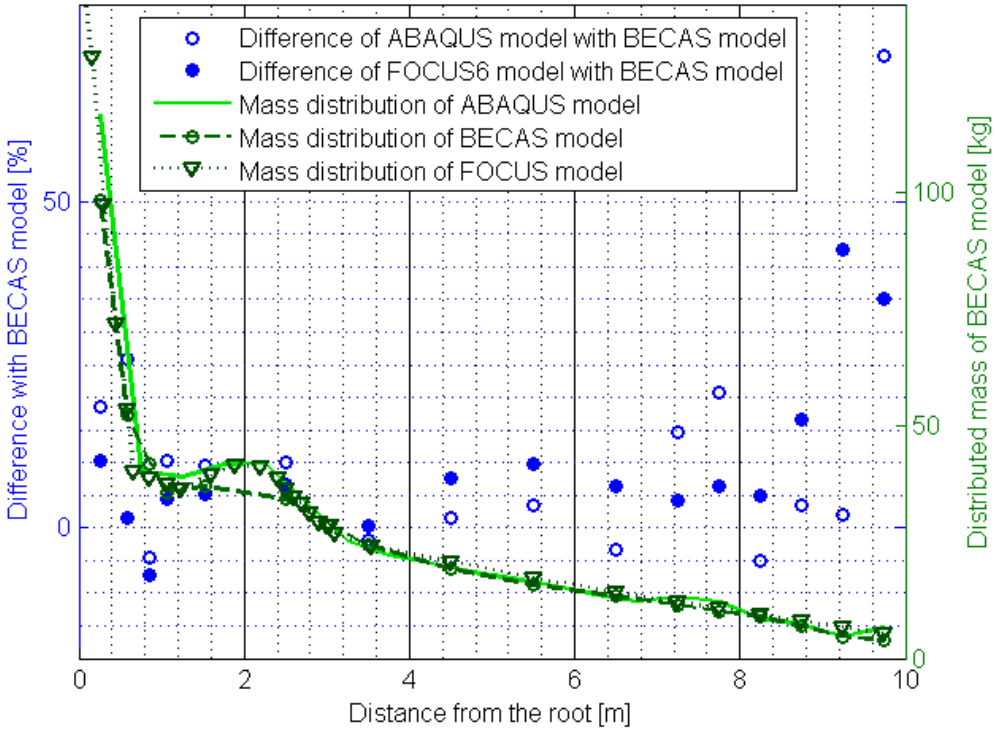

Figure 26 – Absolute blade mass of BECAS, FOCUS6 and ABAQUS model and the difference of ABAQUS and FOCUS6 model w.r.t. BECAS model

Table 9 - Location of the centre of gravity

		BECAS-HAWC2	FOCUS6-HAWC2	ABAQUS	Measurement
Location of the centre of gravity from the root [m]	**Absolute [Hz]**	3.09	3.15	2.85	3.05
	Difference with HAWC2- BECAS [%]		+2%	-8%	-1%

These variations in mass might be due to differences in the model or differences in modelling inputs. Some variations can however be further explained:

- Near the root and between 1.5 and 2.5 m the low number of cross sections in a region with fast changing mass properties causes mass differences.
- The errors near the tip are larger than over the rest of the blade. A dead mass distribution is added to the model to account for non-structural adhesives, balancing weights, over-laminations etc. The contribution of the dead mass to the total cross-sectional mass is higher near the tip and a small difference in the modelling method of this dead mass distribution can result in larger relative differences near the tip.

4.2.4 Stiffness

The distributed stiffness properties of the BECAS model and the FOCUS6 model are compared. The ABAQUS case is not taken into account in this comparison since the distributed stiffness data is not available. Figure 27 shows the flapwise, edgewise and torsional stiffness parameters calculated with BECAS and FOCUS6. The difference of the FOCUS6 stiffness values w.r.t the BECAS stiffness values is shown in Figure 28. The indicated properties are general cross-sectional properties and no specific material properties. These properties are extracted from the HAWC2 structural input file (see section 3.6):

- Flapwise bending stiffness (EI_x): This is calculated by multiplication of the blade modulus of elasticity E and the flapwise area moment of inertia I_x.

$$EI_x[Nm^2] = E\left[\frac{\mathrm{N}}{\mathrm{m}^2}\right] * I_x\,[m^4] \qquad (2)$$

- Edgewise bending stiffness (EI_y). Calculated the same way as EI_x but with the edgewise area moment of inertia I_y.

$$EI_y[Nm^2] = E\left[\frac{\mathrm{N}}{\mathrm{m}^2}\right] * I_y\,[m^4]. \qquad (3)$$

- Torsional stiffness (GJ). This is calculated by multiplication of the blade shear modulus of elasticity G and the torsional stiffness constant J.

$$GJ\left[\frac{Nm^2}{rad}\right] = G\left[\frac{\mathrm{N}}{\mathrm{m}^2}\right] * J\left[\frac{m^4}{rad}\right] \quad (4)$$

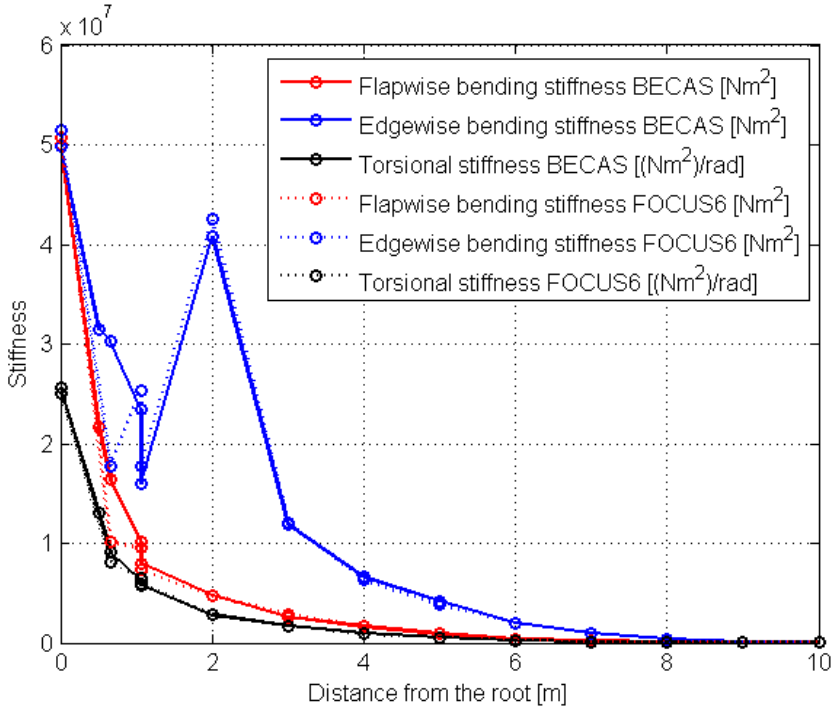

Figure 27 – Distributed stiffness properties calculated with BECAS and FOCUS6

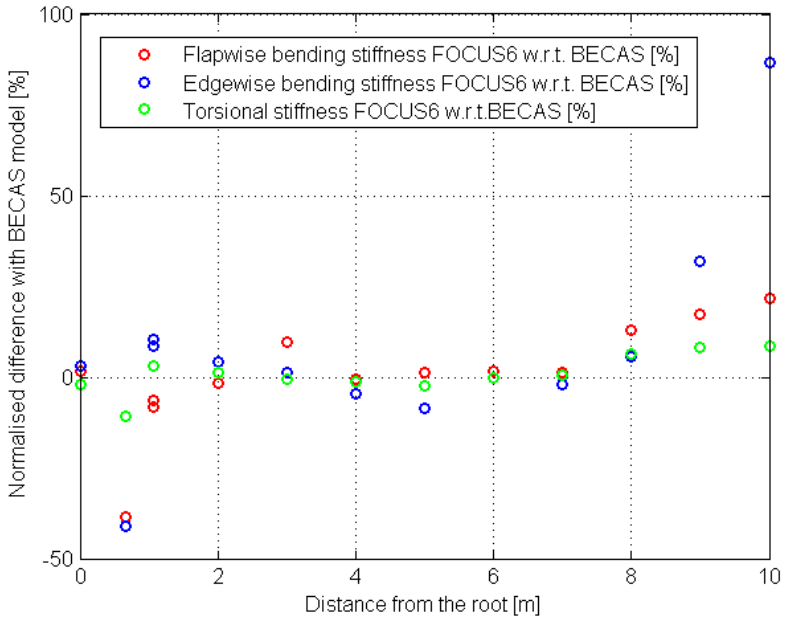

Figure 28 - Difference of the stiffness properties calculated with FOCUS6 w.r.t. the values of BECAS (see Figure 27)

Comparison:

- Overall the three stiffness distributions are similar.
- The FOCUS6 stiffness near the tip is higher than the BECAS stiffness, especially the edgewise stiffness.
- The section at 0.661 m from the root has very high stiffness values for the FOCUS6 case compared with the BECAS case. This can be mainly declared by the low resolution of sections near the root. Numerous ply drops and fast changing contour make that the stiffness values change very fast. A small offset in location may induce a large stiffness difference.

4.2.5 Eigenfrequencies

The eigenfrequencies summarise combined mass and stiffness characteristics and therefore dynamic behaviour. The first flapwise and first edgewise eigenfrequencies for the three structural models are shown in Table 10. The eigenfrequencies cannot only be verified but also be validated with two separate measurements which have been performed on the prototype blade. Only the first edgewise and flapwise eigenfrequencies have been taken into account. To find the other eigenfrequencies is not possible with the current HAWC2 model. A validation of higher order eigenfrequencies is therefore considered out of the scope of this thesis. For future validation procedures, HAWCstab2 is recommended as described in Chapter 7.

Eigenfrequencies (ω_n), mass (m) and stiffness (K) of simple mass-spring systems relate to each other in the following way:

$$\omega_n = \sqrt{\frac{K}{m}} \tag{5}$$

This relation can be applied to the wind turbine blade and explains the ratio between the overall stiffness and mass characteristics. Comparison:

- The first edgewise and flapwise eigenfrequencies of the BECAS and ABAQUS model are very close (< 2 % difference).
- The first edgewise and flapwise eigenfrequencies of the FOCUS6 model are lower than the ones of the BECAS model.
- The flapwise and edgewise eigenfrequencies measurements on the prototype blade w.r.t. the BECAS model behave oppositely. The flapwise frequency is 8 % higher while the edgewise frequency is 7-9 % lower. The total mass measured on the prototype blade is higher (see section 4.2.3). When comparing this with the high flapwise eigenfrequency and the low edgewise eigenfrequency one may conclude that the increase in material is focused on an increase in flapwise stiffness.

Table 10 - Eigenfrequencies of the XANT M-21 wind turbine

		BECAS-HAWC2	FOCUS6-HAWC2	ABAQUS	Measurement
1st flapwise eigenfrequency	Abslute	3.27	3.04	3.32	3.53
	Relative		-7 %	+2 %	+8 %
1st edgewise eigenfrequency	Absolute	6.74	6.14	6.59	6.25
	Relative		-9 %	-2 %	-7 %/-9 %

4.3 Analysis of differences and similarities

A verification procedure has been performed based on three different models. The differences and similarities have been identified in sections 4.2.1 – 4.2.5. These differences and similarities are analysed and combined in this section to come up with conclusions about the accuracy of the current modelling procedure. All models in this comparison are based on the assumption of linear stiffness. Since the XANT M-21 wind turbine has a conventional stiff blade this is considered a valid assumption. If flexible blades are modelled the deviations can be significant which might require a non-linear stiffness approach. This is considered outside the scope of this thesis research. It is addressed in Chapter 7 and Appendix C.

4.3.1 Measurement data

Some measurements are available to use as validation material such as mass, eigenfrequency and centre of gravity. Except for the eigenfrequencies these have a rather significant difference with the modelled values. This can be due to a different reasons. The focus is not on the absolute validation but rather to see if, with the same input data, the model behaves the same as the other models. Therefore these are shown as reference value but not further taken into account in this analysis.

4.3.2 Edgewise behaviour

The edgewise behaviour of the ABAQUS-HAWC2aero model shows some differences with respect to the two HAWC2 models. In the dynamic comparison as well as in the static displacement under tip loading the ABAQUS model behaves more stiff than the other models. The eigenfrequencies are however not affected. The FOCUS6-HAWC2 model behaves very much the same as the BECAS-HAWC2 model when looking at the dynamic and static response and stiffness distribution. The eigenfrequencies are however about 10 % different, which is more than expected regarding the other similarities.

There is no clear explanations for the differences in edgewise direction. The edgewise behaviour is relevant to compare the models but it will not affect the results significantly since the edgewise

behaviour is not critical. Therefore the differences are found to be small enough to consider the edgewise behaviour of the BECAS-HAWC2 model verified.

4.3.3 Flapwise behaviour

The mass, stiffness and eigenfrequencies are similar for the three models. This is clearly seen in the flapwise dynamic and static response. The FOCUS6 case has a difference in flapwise moment and displacement which is also seen in the lower flapwise eigenfrequency. This is mainly due to the higher mass in the outer part of the blade. This higher mass difference is due to different inputs or a difference in the model. For the purpose of this research the flapwise behaviour of the BECAS-HAWC2 model is considered verified.

4.3.4 Torsional behaviour

Some differences in torsional behaviour between the ABAQUS and BECAS-HAWC2 models could be seen from the **static response**. Since the applied moment for the two models is the same there is a difference between the BECAS-HAWC2 structural model and the ABAQUS structural model. This is probably due to the way the structural models (Timoshenko beam model and ABAQUS model) deal with torsion introduced by sweep. As described by [33] shell models such as the ABAQUS model perform very well regarding flapwise bending but over predict the twist angles significantly which might be the cause of this difference.

The **dynamic comparison** shows that a difference in twist loading causes an extra difference in tip twist behaviour which is far more significant than the difference of the static response. Since the aerodynamic properties like power and thrust are the same the probable causes of this difference are the following:

- The moment force is calculated differently due to difference in aerodynamic model. In this case the aerodynamic model of HAWC2 should be more correct than HAWC2aero since HAWC2 is updated more often.
- The moments and forces are introduced in the structural model differently due a difference in the coupling between structural and aerodynamic model. HAWC2 is a validated tool while the ABAQUS-HAWC2aero coupling has just recently been developed and not been extensively validated yet. This twist moment should be further examined but in the current stage of the research the BECAS-HAWC2 model is assumed to be more accurate due to the higher level of validation.

Some subsequent verification options are proposed for further research:

- To check if the difference occurs due to the swept blade planform: compare models without sweep.

- To check if the same moments and forces are calculated: compare the aerodynamic forces and moments directly.
- To check if the difference occurs due to a difference in deflections: model a rigid blade.

4.4 Summary

A verification procedure has been conducted with three different models of the same blade of the XANT M-21. The minor differences between several modelled parameters increase the confidence in the BECAS-HAWC2 model. In flapwise and edgewise direction the results correspond well enough to consider the current BECAS-HAWC2 model verified for the purpose of this research. In torsional direction the differences are too significant to neglect but in the current stage of the research the BECAS-HAWC2 model is assumed to be more accurate due to the higher level of validation.

5 Blade design setup and results

The tool which is described in Chapter 3 is used to design and evaluate flexible blades which is addressed in this Chapter. Several iteration steps are used to come to the best flexible design.

5.1 New blade design

This section describes the location and type of the material which is used to design flexible blades.

5.1.1 Effect of spar cap and skin material

To increase flexibility is a very general thing. Several materials are present in a wind turbine blade, as is discussed in the section 3.1.2, providing specific strength and stiffness. This section focuses on the effect on mass and stiffness of two main materials: the BD blade skin material and the UD spar cap material (see Figure 6). BECAS simulations of a cross section at 75 % of the blade are performed to check what the effect is on the major stiffness properties if these skin and spar cap materials are removed.

These materials are removed by making the structural and mass properties negligible. The differences with the original cross section regarding flapwise bending stiffness (EI_x), edgewise bending stiffness (EI_y), torsional stiffness (GJ) and mass are shown in Table 11.

Table 11 – Change in stiffness and mass properties when considering no spar cap or no skin

	m	EI_x	Ei_y	GJ
No spar cap material	-15 %	**-67 %**	-12 %	-7 %
No skin material	**-42 %**	-31 %	**-95 %**	**-99.9 %**

The following conclusions are made:

- The BD skin material contributes a significant amount of 42 % to the total cross-sectional mass while the UD spar cap material contributes only 15 %.
- The flapwise bending stiffness reduces with 67 % without the UD spar cap material from which it is concluded that the spar cap provides the main part of the bending stiffness.
- The edgewise and torsional stiffness are reduced with 95 % and 99.9 % respectively without the skin material. Therefore the conclusion is made that the skin material provides the torsional stiffness and the edgewise bending stiffness.

To change the flapwise bending stiffness of a blade the UD spar cap material should be adapted while a reduction in torsional stiffness is completely covered by the BD skin plies. These results are used to design the new flexible blades in sections 5.1.4 - 5.1.6.

5.1.2 Wind turbine blade materials

Information about the current wind turbine blade materials is addressed in this section. Currently wind turbine blades are made of fibre-reinforced polymers. The fibres provide the required longitudinal stiffness and strength while the resin matrix material is responsible for the fracture toughness, delamination strength and out-of-plane strength and stiffness. These materials are commonly assumed to behave linear elastically which is in general a valid assumption due to the relatively low deformations.

Regarding the fibres, mostly E-glass fibres are used, which are cheap and widely available. Other fibres are developed for wind turbine blades which have higher specific strength, stiffness or fatigue properties however these are seldom used in practice. These comprise S-glass fibres, carbon fibres, basalt fibres, aramid fibres etc. However these all come at a higher cost. The matrix material is mostly a thermoset material such as epoxy, polyester or vinylesther. More seldom thermoplastics are used of which the most important advantage is the recyclability, these can be melted and reused when heated [34].

5.1.3 Selection of flexible 3D material properties

This section describes the flexible material properties used to design flexible blades and how these are determined. In the current modelling procedure a material ply is assumed to have homogeneous, anisotropic structural properties and linear elastic behaviour.

Flexible base ply

A new flexible material ply is developed by an external partner. Material tests are performed to find the general stiffness parameters shown in Table 12. This base ply has fibres in the longitudinal direction as shown in Figure 29. This ply is used to generate new laminates by combining several plies in different orientations. When a material is isotropic, only three elastic constants are needed to define the material stiffness properties: tensile modulus (E), shear modulus (G) and Poisson coefficient (ν). When using an anisotropic material however these stiffness parameters can be different for the three directions.

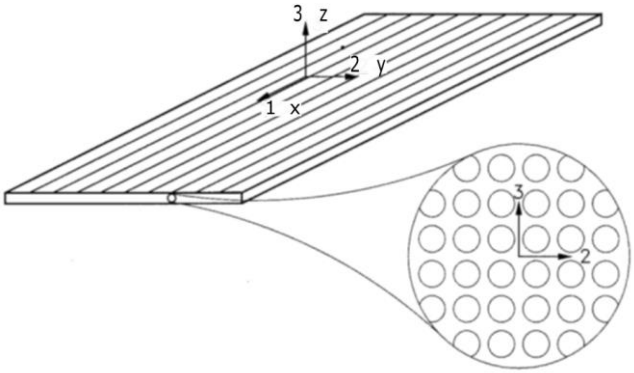

Figure 29 – Schematic image of the unidirectional base ply and the principle ply directions [35]

The ply is assumed to behave transversely isotropic which means that the properties in the plane transverse to the fibre direction are isotropic (see Figure 29) which results in the following simplifications of the material properties [35]:

- $E_{22} = E_{33}$
- $G_{12} = G_{13}$
- $\nu_{12} = \nu_{13}$
- $\nu_{23} = \nu_{32}$

Some material properties of the new material have been found from tests, others have been calculated as can be seen in Table 12. Based on findings from Lagace [36] G_{23} is assumed to be $0.8*G_{12}$. The most important values are the in-plane properties, which are highlighted in Table 12, since most loading will be in-plane loading.

Table 12 - Stiffness parameters for unidirectional base ply

	Original UD ply/laminate properties	**Origin**	**Flexible UD ply properties**	
	absolute value		*absolute value*	*relative w.r.t. original UD ply material*
E_{11} [MPa]	40 140	*measured*	10 125	-75%
E_{22}[MPa]	12 950	*measured*	89	-99.3%
E_{33} [MPa]	12 950	*transversely isotropic*	89	-99.3%
G_{23}[MPa]	3 490	*Lagace* [36]	22.4	-99.4%
G_{13}[MPa]	3 490	*transversely isotropic*	28	-99.2%
G_{12}[MPa]	5 941	*measured*	28	-99.5%
ν_{12} [-]	0.28	*measured*	0.4	43%
ν_{13} [-]	0.09	*transversely isotropic*	0.4	344%
ν_{23} [-]	0.09	*highly flexible material*	0.49	444%
ρ [kg/m^3]	1 920	*measured*	2 813	47%

Flexible Laminates – Software Kolibri

A laminate is a stack of different plies as can be seen in Figure 30. The base ply described in the previous section is used as base to design three different laminates:

- **UD laminate**: UD base plies are stacked together, all plies in lengthwise direction without any rotations, to form a UD laminate.
- **BD +/-45 deg laminate**: The unidirectional UD base ply is rotated 45 deg and is used as a base to form a +/-45 deg laminate with alternating a +45 deg ply and a -45 deg ply.
- **BD 0-90 deg laminate**: The UD base ply is stacked with alternating a 0 deg ply and a 90 deg ply to form the the 0-90 deg laminate.

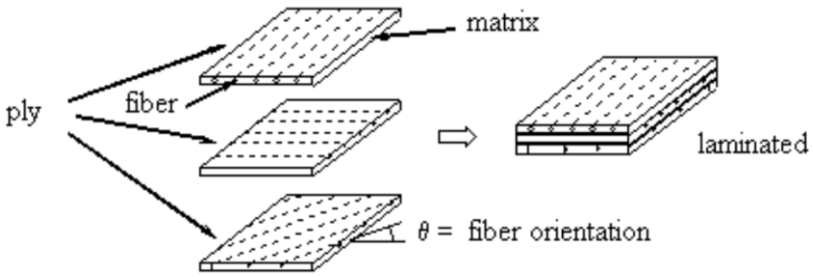

Figure 30 – Design of the laminate from the base ply [37]

The software Kolibri is used to calculate the stiffness properties of these laminates (see Table 13). Kolibri is a design and analysis tool for composite materials and structures [38]. It is based on classical lamination theory which is an extension of the classical plate theory to composite laminates. More information on this theory can be found in [39]. The Kolibri version 2.3 is used.

The most important values are the in-plane properties since most loading will be in-plane loading. Therefore these properties are highlighted in Table 13. The classical lamination theory of Kolibri uses only in-plane properties. BECAS however uses the out-of-plane properties as well in the calculations. Since the fibres will not have a significant contribution to the stiffness in the out-of-plane direction the assumption is made that the out-of-plane stiffnesses (G_{13}, G_{23} and E_{33}) and Poisson coefficients (ν_{13} and ν_{23}) of the laminates will stay the same as these of the UD ply.

Table 13 – Stiffness parameters for ply and lamina

	Original +/- 45 deg BD laminate	Flexible +/- 45 deg BD laminate		Flexible 0-90 deg BD laminate	
		absolute value	relative w.r.t. original skin	absolute value	relative w.r.t. original skin
Rotation angle [deg]		+/-45		0-90	
E_{11} [MPa]	12 900	110	0.85%	5 062.50	39%
E_{22}[MPa]	12 900	110	0.85%	5 062.50	39%
E_{33} [MPa]	12 000	89	0.74%	89	0.74%
G_{23}[MPa]	5 860	22.4	0.38%	22.4	0.38%
G_{13}[MPa]	11 000	28	0.25%	28	0.25%
G_{12}[MPa]	11 000	2 539	23%	28	0.25%
ν_{12} [-]	0.55	0.98	178%	0.007	1.27%
ν_{13} [-]	0.1	0.4	400%	0.4	400%
ν_{23} [-]	0.1	0.49	490%	0.49	490%
ρ [kg/m^3]	1 920	2 813	47%	2 813	47%

The material properties described in Table 12 and Table 13 are used to generate several structural input files for HAWC2. Three basic cases are considered where a part of the material is changed with a flexible material type while all other materials remain the same:

- The skin is replaced with the flexible BD +/- 45 deg laminate .
- The skin is replaced with the flexible BD 0 – 90 deg laminate.
- The full spar cap is replaced with the UD laminate.

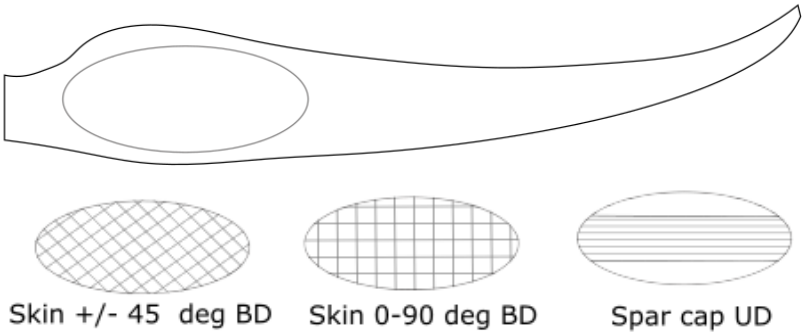

Figure 31 – Three different blade designs with flexible ply

These three cases result each in a very different structural blade. The structural and mass properties of these three adapted blades are shown in shown in Figure 32. The values are normalised w.r.t. the original unchanged blade properties. Making the skin flexible increases the mass more than by making the spar cap flexible since the skin contains more material than the spar cap. The density of the three different flexible material types is the same.

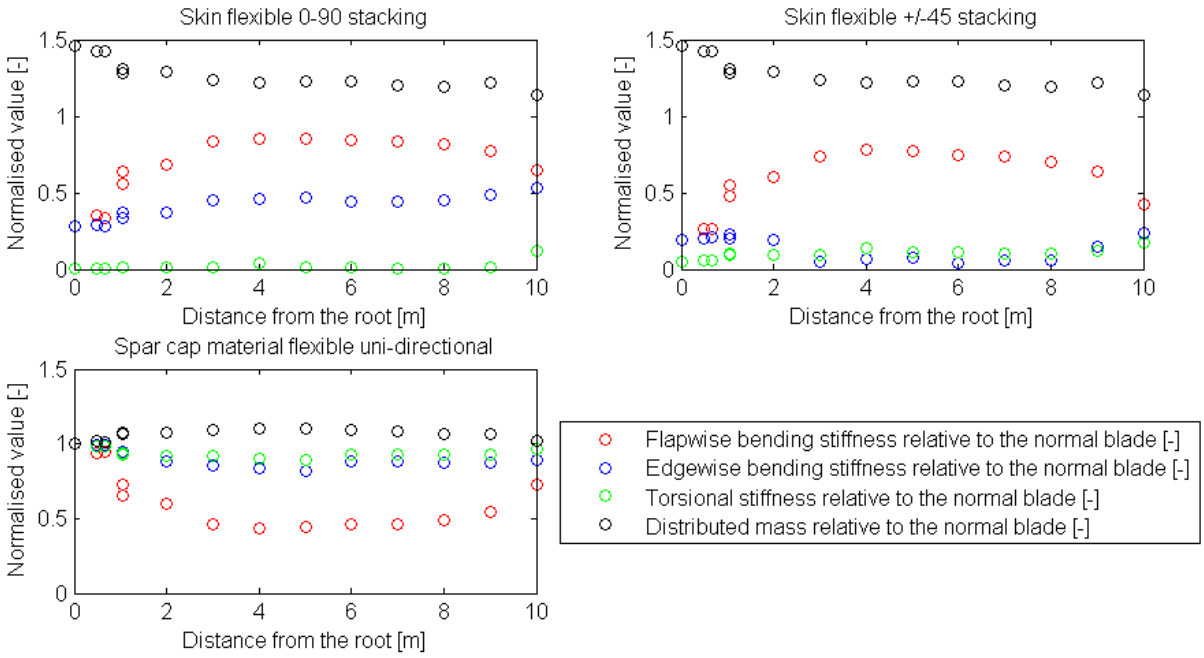

Figure 32 - The structural and mass properties of three adapted blades: the skin is replaced with the flexible +/- 45 deg laminate (top right) or the 0 – 90 deg laminate (top left) or the full spar cap is replaced with the unidirectional ply (bottom). The values are normalised w.r.t. the original unchanged blade properties.

5.1.4 Change the skin with flexible 0-90 deg laminate

The complete skin is made flexible, also the unidirectional material in the root is changed with the UD flexible ply material. As can be seen in Figure 32 this results in very low torsional stiffness all over the blade. This is as expected since there are no fibres restraining torsional movement and all the torsional moments are taken by the matrix material only. Since it is the skin material which provides torsional stiffness (see section 5.1.1) it is the in-plane shear stiffness of the 0 – 90 deg ply material which determines the torsional stiffness. As can be seen in Table 13 this in-plane shear stiffness is reduced with 99.52 % which clarifies the very significant reduction in torsional stiffness.

5.1.5 Change the skin with flexible +/-45 deg laminate

Figure 32 shows that this results in a very low edgewise bending stiffness. Also the torsional stiffness is reduced but not as much as when the 0-90 deg laminate is used in the skin. This edgewise bending stiffness is provided by the skin (see section 5.1.1) which again should be provided by the Young's modulus in lengthwise direction. This lengthwise Young's modulus is significantly reduced with 99.15 % compared to the original skin material (see Table 13).

5.1.6 Change the complete spar cap with flexible unidirectional laminate

Figure 32 shows that changing the spar cap material to the flexible unidirectional laminate affects mainly the flapwise bending stiffness. The spar cap provides the main contribution to the flapwise bending stiffness (see section 5.1.1). It is therefore the lengthwise Young's modulus which provides the stiffness which is reduced with 75 % compared to the original blade (see Table 12).

5.2 Key performance indicators

The three main output parameters which are described in section 3.7 are the stability, annual energy yield (AEY) and maximum loading which is the maximum thrust force ($F_{T,max}$) and the maximum root bending moment ($M_{root,max}$). If the case is instable it is not considered. The maximum loading and energy yield however should be respectively as low and as high as possible. In the results in the following sections the combined relative parameter is also considered: maximum loading divided by energy yield or "load-of-energy". This is similar to the "cost-of-energy" but since the cost is not considered in this research and the optimisation is focussed on the load, the "load-of-energy" parameter is used to capture the reduction in loading and energy increase in one parameter. All parameters are presented with their abbreviation and desired trend in Table 14.

Table 14 – Key parameters for evaluations including parameter abbreviation and the desired trend

Parameter	Parameter abbreviation	Desired trend
Annual energy yield	AEY	High
Maximum thrust force	$F_{T,max}$	Low
Maximum root bending moment	$M_{root,max}$	Low
Maximum thrust force divided by annual energy yield	$F_{T,max}$ /AEY	Low
Maximum root bending moment divided by annual energy yield	$M_{root,max}$/AEY	Low

5.3 Results

The new flexible blade designs described in section 5.1 are simulated with HAWC2 and further optimized in this section to find the best flexible design. The different simulation steps are summarized in Table 15. This table shows how the different design results perform regarding AEY and maximum loading. Also the next steps in the simulation procedure are shown. The following sections describe these results in more detail.

Table 15 – Simulation steps to find best flexible design. Red shows negative results, green shows positive results.

Simulation steps	Flexible material	Stable	AEY	$F_{T,max}/M_{root,max}$	Next steps
I: Flexible material in full blade	Spar cap UD	Yes	0%	-4%/-7% (not enough)	Not further considered
	Skin +/- 45	No	/	-1%/-3%	Change design
	Skin 0-90	No	/	-21%/-31%	Change design
II: Partial flexibility 1	Skin +/- 45	Yes	No increase	No reduction	Not further considered
	Skin 0-90	Yes	Increase	Reduction	More detailed analysis
III: Partial flexibility 2	Skin 0-90	Yes	+11%	-23%/-26%	Further iteration
IV: Partial flexibility 3	Skin 0-90	Yes	+11%	-23%/-26%	Best Flexible Design

Step I: Flexible material in full blade

The full blade is changed with the three flexible materials and the results are shown in Table 15.

Change spar cap with flexible UD laminate

The annual energy yield (AEY) remains the same while the maximum thrust force ($F_{T,max}$) reduces slightly (-4 %) as does the maximum root bending moment ($M_{root,max}$) (- 7%). This is not considered significant enough for the purpose of this research and is therefore not further considered.

This is the only case which focusses specifically on reducing the bending stiffness. The +/-45 deg and 0-90 deg laminate materials are not used in the spar caps since the assumption is made that these materials will not be able to cope with the high flapwise bending loads.

Change skin with flexible BD 0-90 deg laminate

This flexible case results in a significant reduction in extreme loading. The flexible BD 0-90 skin material reduces the $F_{T,max}$ with 21 % and the $M_{root,max}$ with 31 %. The AEY could not be calculated yet since the blade had divergent unstable behaviour in the higher wind regimes. Further research is performed on this case.

Change the skin with flexible BD +/-45 deg laminate

No significant reduction in $F_{T,max}$ (-1 %) and $M_{root,max}$ (-3 %) could be seen. The power could not be analysed due to instabilities and therefore further research is performed on this case.

Step II: Partial flexibility 1

The blades with flexible material in the full blade skin are unstable. Therefore the blade is lengthwise divided in different parts and only one section is made flexible at the time. The blade has been divided

in two, three, seven and 14 cross sections as can be seen in Figure 33. These partial flexible blades are analysed.

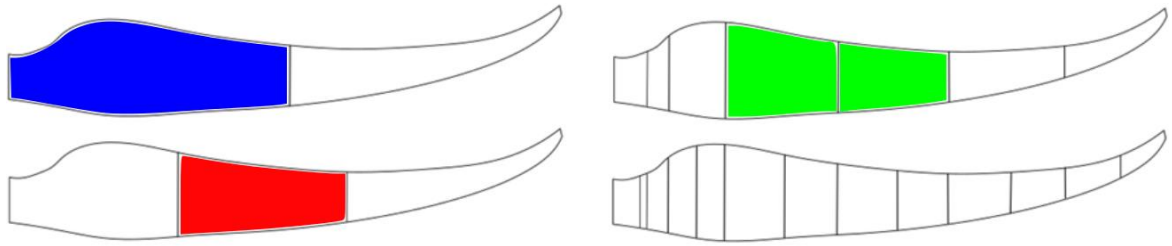

Figure 33 - The blade is divided in two, three, seven and 14 cross sections. One by one each of these cross sections is made flexible. The coloured sections indicate which skin sections should be changed with BD 0-90 deg material to reduce the load-of-energy with more than 5 %.

$M_{root,max}$ and $F_{T,max}$ are plotted together with the AEY in Figure 34, all relative to the original blade. Only the stable simulations are included in this plot. The blades with 0 - 90 deg flexible material have much better results than the blades with +/- 45 deg flexible material when considering maximum loading or increase in AEY. Some blades with 0-90 deg flexible material have a significant reduction in loading combined with an increase in AEY. The focus will therefore be on the cases with 0 – 90 deg flexible material only, the +/- 45 deg flexible material in the skin is not further considered in this research.

Recalling the results of the literature research in Chapter 2 these results are not unexpected. By reducing the torsional stiffness of a blade which has a swept planform such as the XANT M-21 it is the bend-twist coupling which is increased. Under the same loading the blade twist increases. This increase in bend-twist coupling can reduce the maximum loading as well as increase the energy yield.

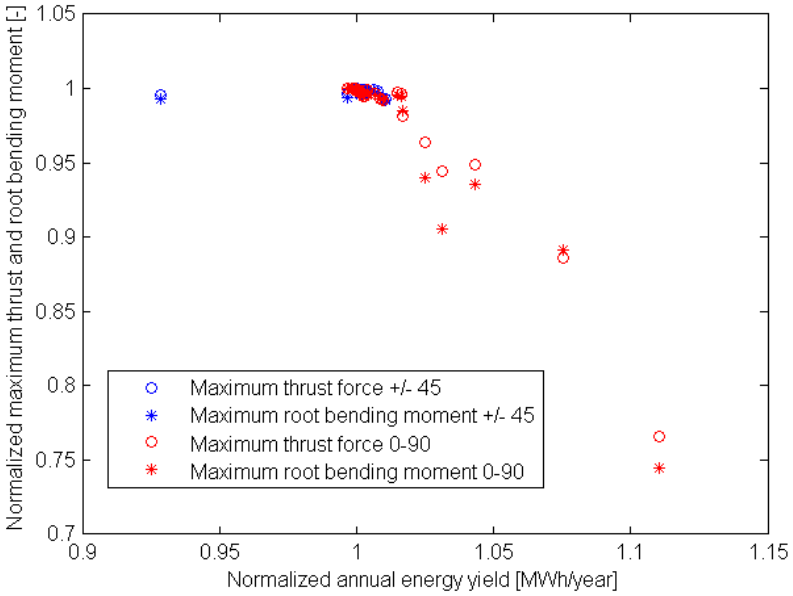

Figure 34 – Maximum thrust, maximum root bending moment and annual energy yield of blades partially made of +/- 45 deg and 0-90 deg flexible blade material

Step III: Partial flexibility 2

Figure 35 is based on the same data as the previous section with only the cases with the 0–90 deg flexible skin material considered. This figure shows the AEY, $F_{T,max}$ and $M_{root,max}$ for different structural designs where in every case one part of the blade is made flexible. The legend shows how long the flexible part is (also shown in Figure 33). The horizontal axis shows the location of the middle of the flexible section. To visualize these results the cases where the load-of-energy reduction is above 5 % are shown in Figure 33 in the colour corresponding to Figure 35. Some conclusions are drawn:

- If a large part near the tip is made flexible the blade behaves unstable. The unstable cases are not shown in Figure 35 and are not further taken into account in this research.
- In general the first 5m of the blade is the best part to introduce flexible skin material regarding the increase in AEY as well as the reduction in $F_{T,max}$ and $M_{root,max}$.
- One case performs significantly better than all others. This is the case where the skin of the blade is made flexible starting from the root up to 5 meter from the root (see blue part of the blade shown in Figure 33). This case is further addressed in the following step in the results.

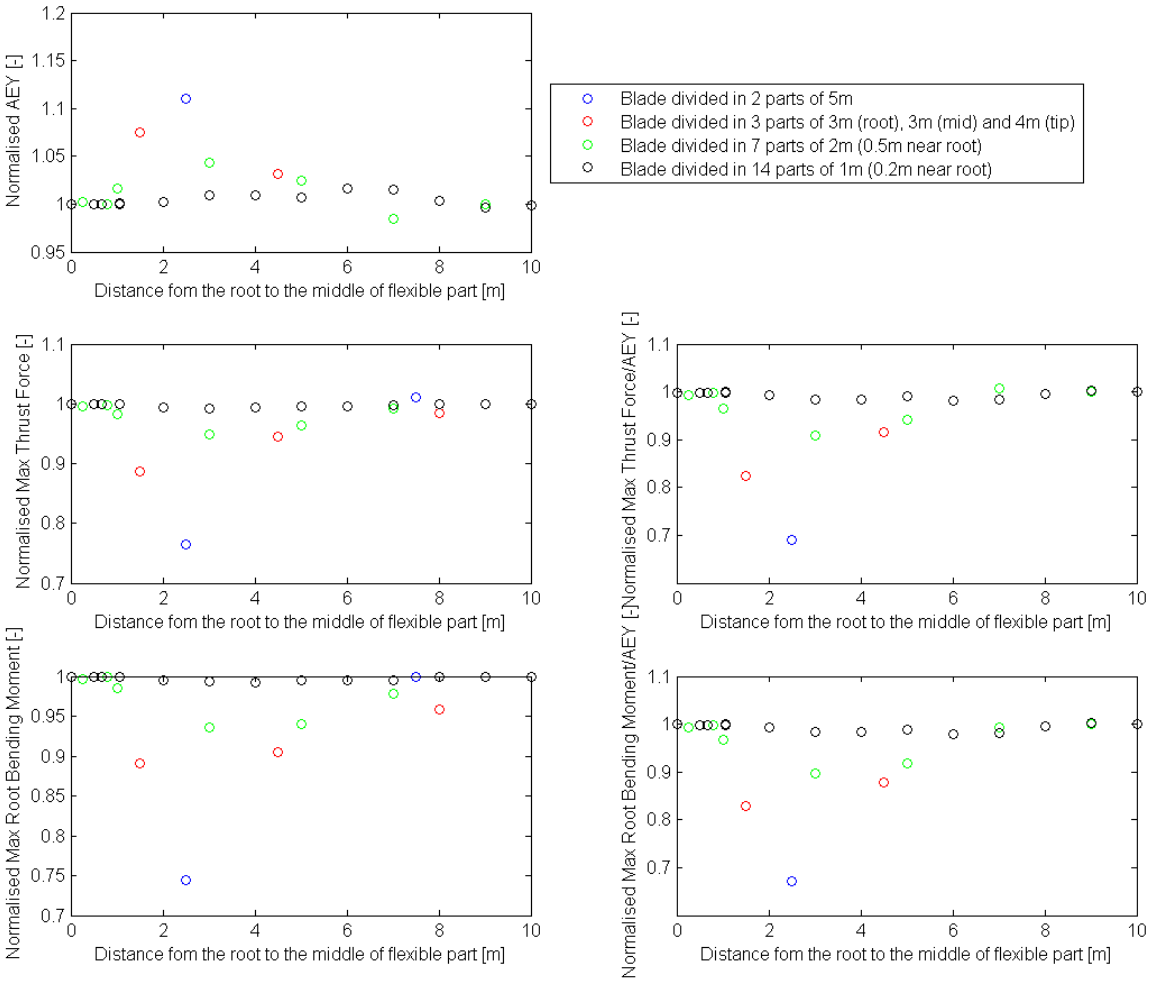

Figure 35 – The skin is replaced with flexible +/- 90 deg material. Only a part of the blade is made flexible.

Step IV: Partial flexibility 3

As shown in the previous section replacing the skin with BD 0-90 deg flexible material from the root to the middle of the blade performs best. To further explore the best options this same case is considered but the location where it changes from flexible to the original material is changed in steps of one meter (see Figure 36). Smaller steps are not possible with the current model. Figure 37 shows the variation of the key performance indicators when changing the length of the flexible root part. The $M_{root,max}$ shows very similar results with the $F_{T,max}$ and is therefore not shown. Some conclusions:

- Increasing the flexible root part increases the AEY and reduces $M_{root,max}$ and $F_{T,max}$.
- Making the flexible part longer than 5m results in instable behaviour and significant reduction in AEY.
- A flexible part of 5m starting from the root is still the best: the lowest $M_{root,max}$ and $F_{T,max}$ as well as the highest AEY. Therefore this case is called the "best flexible design". The main energy and loading characteristics of this case are summarized in Table 16.

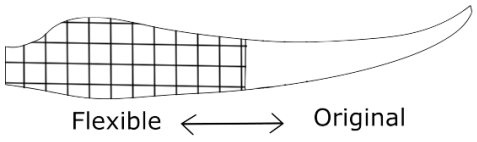

Figure 36 – Length variation of the flexible part with 0-90 deg flexible laminate in the skin

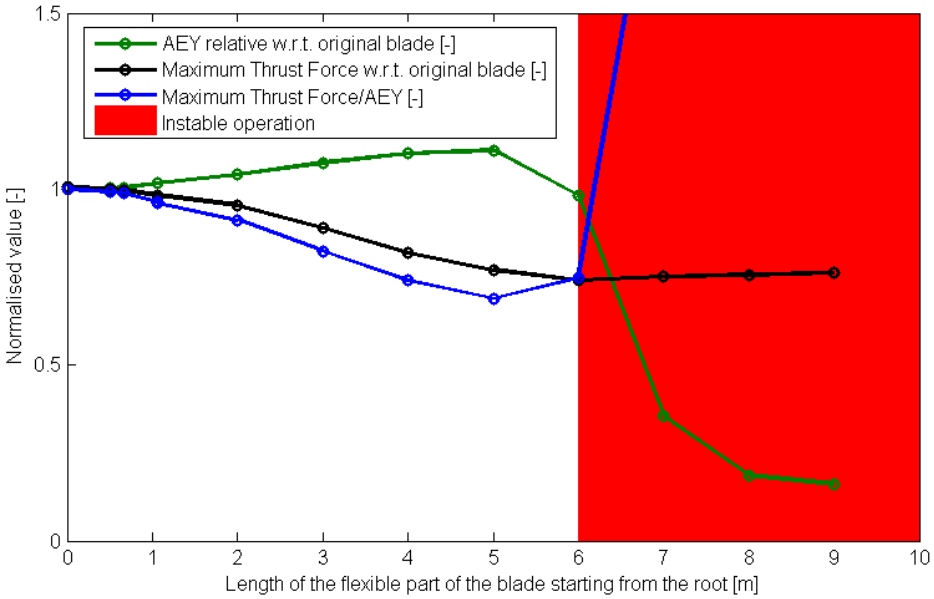

Figure 37 - Change in annual energy yield, maximum thrust force and the ratio between these two by varying flexible root length

Table 16 – Main energy and loading parameters from original and new flexible blade

	Original blade	Best flexible design	Difference of new w.r.t. original blade [%]
AEY [MWh/year]	581.9	646.2	+11%
$F_{T,max}$ [kN]	79.6	61.0	-23%
$F_{T,max}$/AEY $\left[\frac{kN}{MWh/year}\right]$	0.14	0.09	-31%
$M_{root,max}$ [kNm]	110.8	82.3	-26%
$M_{root,max}$/AEY $\left[\frac{kN}{MWh/year}\right]$	0.19	0.13	-33%
Maximum change in tip twist [deg]	4.6	52.4	+1039%

5.4 Summarizing analysis of best flexible design

In this research a blade is designed which is able to reduce the extreme loading considerably combined with a significant increase in energy production. This section addresses the main limitations which are taken into account. The increase in AEY and the reduction in loading are further explained.

5.4.1 Limitations

Reducing the torsional stiffness works best to reduce the loads and to increase the energy yield. This reduction in torsional stiffness increases the bend-twist coupling of the blade. The good results regarding load reduction and energy increase are both confirmed by results from literature (see Chapter 2).

Flexible blades can be designed in many different ways. To limit the scope the design process includes:

- three flexible material laminates
- three main material types of which the properties are changed
- 14 different lengthwise blade positions in which flexibility is introduced

The best flexible design is a preliminary design. Before the first highly flexible wind turbine is build more research is needed. Many things such as manufacturability, maximum allowed strain, buckling, stability in all load cases, the validity to assume linear materials etc. have to be examined (see Chapter 7). Options regarding non-linear behaviour are further addressed in Appendix C. The current best flexible design is however an indication of:

- the type of materials which allows for this level of deformation
- the blade location in which these type of materials should be used
- the level of load reduction and energy increase which can be achieved

5.4.2 Increase in annual energy yield

All energy comes from the increased performance in the higher wind regimes (see Figure 38). From 12 m/s and higher the best flexible design performs better than the original blade. The power curve of the flexible case looks similar to this of a pitch controlled wind turbine.

The AEY for different wind speeds is shown in Figure 39. This figure shows that indeed the increase in AEY of 11 % is found between 12 and 20 m/s.

The blades of stall controlled wind turbines are designed such that in high wind speeds stall occurs and the power as well as maximum rotor torque decreases so that the wind turbine can cope with these loads. When the best flexible design is considered the power stays close to a certain maximum in the higher wind regimes. The blade does not stall the same way as the original blade, the winds speed where stall of the blade occurs is delayed due to the reduction in angle of attack under higher loading. This is due to the twist-to-feather motion of the blade (see Figure 40). The power behaviour is close to the behaviour of a pitch controlled wind turbine but is achieved in a passive manner without active pitching system. This effect is confirmed by literature (see section 2.3). The maximum operational blade twist is found in literature to be 30 – 40 deg to have passive power control [11] while the best

flexible design of this research has a maximum operational tip twist of only 5 deg. This is probably due to the centrifugal stiffening effect which is not present in the case from literature.

These AEY calculations are performed with an average wind speed of 10 m/s which is taken from the design standards. It will however often occur that a wind turbine is used on a location with a lower wind regime. In this case the increase in AEY will be smaller since all the significant gain in energy is located in the higher wind regimes.

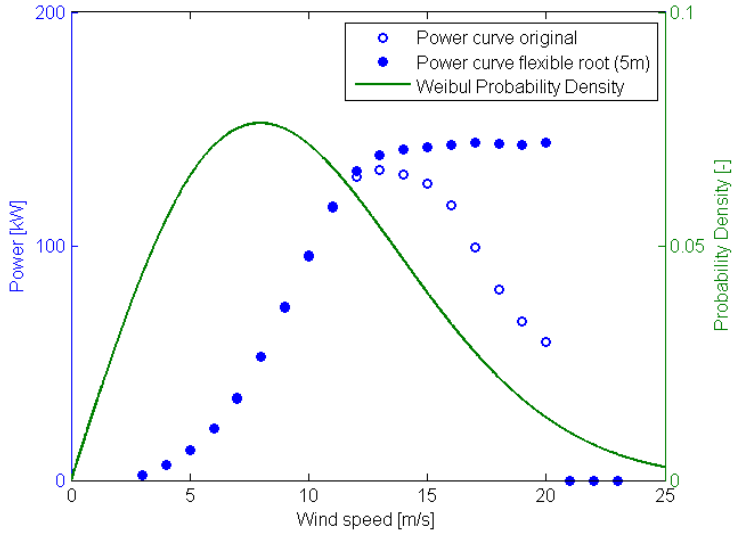

Figure 38 – Power curve, original and flexible root (5m) and Weibull probability density distribution for 10 m/s average wind speed

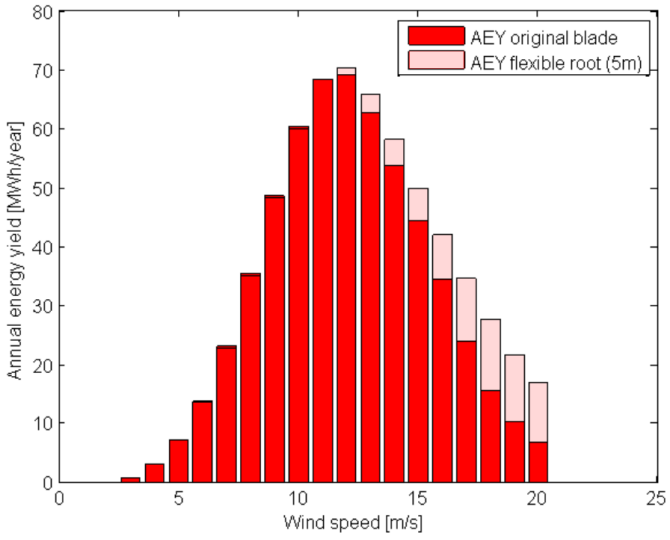

Figure 39 – AEY for different wind speeds of the original blade and the best flexible design

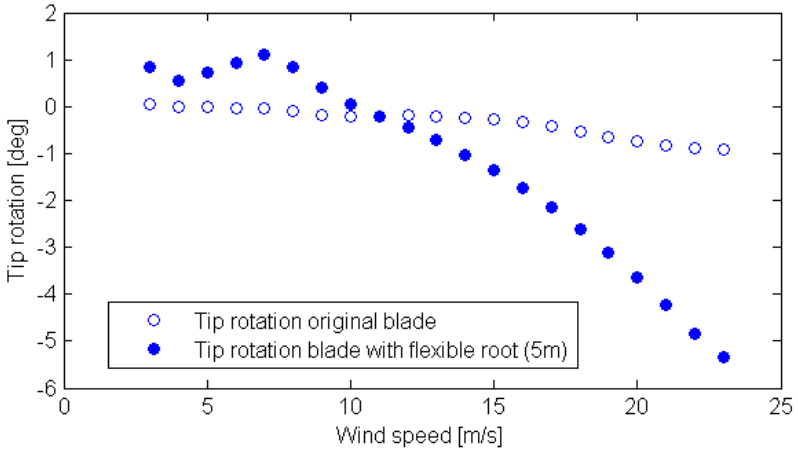

Figure 40 – Tip twist of the original blade and the new flexible blade

5.4.3 Reduction in loading

The best flexible design shows a significant reduction in maximum loading. In this maximum load condition where the wind turbine is parked in a wind speed of 70 m/s the tip twist to feather is found to be 4.6 deg for the original blade and 52.4 deg for the best flexible design (see Table 17). Figure 41 shows the twist distribution over the blade. This significant increase in twist of the blade is located nearly all in the first half of the blade where the flexible material is used. This explains the reduction in maximum loading: the frontal area of almost the complete blade is reduced due to the blade twist.

Table 17 – Tip twist under extreme loading

	Maximum change in tip twist
Original blade	4.6 deg
Best flexible case	52.4 deg
Difference of new/original	+ 91 %

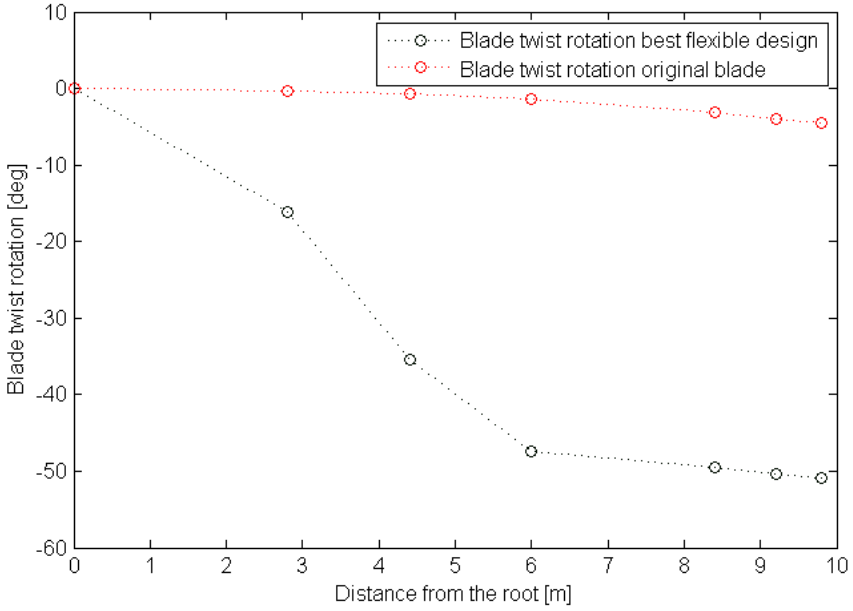

Figure 41 - Blade twist over the length of the blade, stand still under 70 m/s steady wind speed

6 Conclusions

The aim of this research is to design a blade with flexible materials in order to reduce the peak loads on wind turbine blades without compromising the power production.

The **research methodology** which is used to come to the best flexible design is a three-step approach:

- Firstly a modelling tool is created to design and evaluate blades with new flexible materials at different locations in the blade.
- Secondly a verification procedure is performed to check the accuracy of the modelling tool.
- Thirdly this tool is used to design blades with highly flexible materials and to perform an analysis of these new blade designs.

The **modelling tool** is based on the cross sectional software BECAS to design new flexible blades and on the aeroelastic software HAWC2 to analyse the behaviour. This BECAS-HAWC2 modelling tool is based on the existing XANT M-21 wind turbine of which only the blade materials are variable parameters, the rest of the wind turbine remains the same.

The **verification procedure** compares the modelling tool with two other models of the same blade: a FOCUS6-ABAQUS and an ABAQUS-HAWC2aero model. The minor differences between several modelled parameters increase the confidence in the BECAS-HAWC2 model:

- In flapwise and edgewise direction the dynamic behaviour of all three models corresponds well enough to consider the model verified.
- The same accounts for the power curve and rotor thrust.
- In torsional direction the dynamically modelled blades have a twist difference between the HAWC2 models and the ABAQUS-HAWC2aero model due to a difference in applied twist moment. This twist moment should be further examined but in the current stage of the research the BECAS-HAWC2 model is assumed to be more accurate due to the higher level of validation.
- The HAWC2 structural beam model and the ABAQUS structural shell model calculate the twist in the blade differently. These differences are considered negligible since the twist variations due to the differences in applied twist moment results in a difference which is multiple times larger.

Let us recall the main research question as stated in the introduction:

How should the different materials in the layup of a swept wind turbine blade be designed by making use of flexible materials in a way that the maximum loading decreases with more than 10 % without compromising the energy yield?

A flexible matrix material with stiff reinforcing fibres is used to **design** different flexible blades. These blades are **evaluated** based on the reduction of the maximum loading (thrust force and root bending moment) and the increase in annual energy yield:

- The spar cap is replaced with the unidirectional ply: no significant improvement regarding maximum loading or energy yield.
- The skin is replaced with the flexible bidirectional +/- 45 deg laminate: no significant improvement regarding maximum loading or energy yield.
- The skin is replaced with the flexible bidirectional 0 – 90 deg laminate: reduction in maximum loading and increase in annual energy yield shows very promising results.

In the iteration procedure the flexible bidirectional 0 – 90 deg laminate is used in different locations of the blade to find the *best flexible design.* This results in a flexible skin material from the root to the middle of the blade:

- Maximum thrust force and flapwise root bending moment of the best flexible design reduces with respectively 23 % and 26 %. This is due to a significant blade twist of up to 52.4 deg at the tip.
- The annual energy yield is not compromised, it even shows a considerable 11 % increase. This is due to a stall delay effect which is caused by a reduction in angle of attack in high wind speeds.
- Both reduction in loading and increase in energy are due to the increase in bend-twist coupling in the blade. This bend twist coupling is caused by the combination of a reduction in torsional stiffness and the swept planform of the blade.
- Both the reduction in maximum loading and increase in annual energy yield are confirmed by results from literature.

The best flexible design is a preliminary design that shows promising results. These results show that by using flexible materials in the blade skin a significant load reduction is combined with an increase in energy. This indicates an untapped potential for future wind energy which makes further research on this topic recommended.

7 Recommendations for future work

The major recommendations for future work regarding this research are the following:

- **More elaborate stability analysis**: The stability analysis used to find the best flexible design is simplified. A more elaborate aeroelastic analysis can be performed by including more load cases to check if the blade remains stable. A redesign towards higher blade stiffness will be needed if this is not the case. Another way of performing this stability analysis is to use modal analysis. HAWCstab2 is a modal analysis tool which can indicate instable behaviour of the new HAWC2 blade models. The input is similar to the input of the HAWC2 model which makes it a convenient tool for this research. This modal analysis can be performed very fast and can find instabilities which are not found with an aeroelastic analysis.
- **Detailed strength analysis:** The flexible blade material results in high strain values. To check if the material can take these strains the stress and strain recovery function of BECAS can be used. By applying the expected maximum loading on the blade, BECAS calculates the corresponding stresses and strains in the blade. If the allowable stress or strain is available this can be used to check if the maximum stress or strain in the material is not exceeded. Also a buckling analysis is not included yet which is very crucial when going to flexible skin materials. The ABAQUS shell model could be used for this.
- **Nonlinear material modelling**: Once the design of a flexible blade goes to a higher level the assumption of linear stress-strain behaviour will not be sufficient and the material nonlinear behaviour should be taken into account. Appendix C describes an example and some challenges related to nonlinear material modelling.
- **Load reduction to cost relation:** By reducing the peak loads many components of the wind turbine such as the blade hub, tower, foundation, etc. can be downsized and therefore the wind turbine can be made cheaper. This relation is however very complicated. Another way of relating load reduction to cost is to increase the blade length thereby increasing the energy yield while keeping the loading the same as the original blade (see Appendix E).
- **Manufacturability**: The manufacturability of this flexible blade is a design parameter which is not yet considered and should be taken into account if the flexible blade is further developed.

8 Bibliography

[1] S. Starckx, “Flemish company finds and masters niche with windmill-in-a-box,” 2015. [Online]. Available: http://www.flanderstoday.eu/innovation/flemish-company-finds-and-masters-niche-windmill-box. [Accessed: 10-May-2015].

[2] IEC, “International Standard IEC 61400-1 third edition,” Commission Electrotechnique Internationale, Geneva, 2005.

[3] M. Rosemeier, “Non-linear Ultimate Limit State Analysis of a Wind Turbine Blade,” DTU Wind Energy, 2013.

[4] D. Verelst, “Graduation report Flexible wind turbine blades: a FEM-BEM coupled model approach,” Delft University of Technology, 2009.

[5] W. C. De Goeij, M. J. L. Van Tooren, and A. Beukers, “Implementation of bending-torsion coupling in the design of a wind-turbine rotor-blade,” *Appl. Energy*, vol. 63, 1999.

[6] S. Larwood and M. Zuteck, “Swept Wind Turbine Blade Aeroelastic Modeling for Loads and Dynamic Behavior,” 2006.

[7] M. Zuteck, “Adaptive Blade Concept Assessment : Curved Planform Induced Twist Investigation,” MDZ Consulting, Texas, 2002.

[8] P. Veers, G. Bir, and D. Lobitz, “Aeroelastic Tailoring In Wind-Turbine Blade Applications,” American Wind Energy Association Meeting and Exhibition, Bakersfield, California, 1998.

[9] D. W. Lobitz and P. S. Veers, “Load Mitigation with Bending/Twist-coupled Blades on Rotors using Modern Control Strategies,” *Wind Energy*, vol. 6, no. 2, pp. 105–117, Apr. 2003.

[10] D. J. Malcolm and A. C. Hansen, “WindPACT Turbine Rotor Design Study,” National Renewble Energy Laboratory, 2006.

[11] A. T. Lee and R. G. J. Flay, “Compliant blades for wind turbines,” University of Auckland, 1995.

[12] S. Reijniers, “Assessment of wind turbine blade materials: methodology,” Delft University of Technology, 2014.

[13] J. Holierhoek, “AE4W21: Wind turbine aeroelasticity: Wind turbine instabilities and resonances,” Delft university of Technology, 2013.

[14] S.J.Hulshoff, *Aeroelasticity, Course Reader*. Delft University of Technology, 2011.

[15] EWEA, “Wind energy’s frequently asked questions,” 2014. [Online]. Available: http://www.ewea.org/wind-energy-basics/faq/.

[16] DNV/Riso, “Guidelines for Design of Wind Turbines,” Det Norske Veritas, Copenhagen and Wind Energy Department, Risø National Laboratory, 2002.

[17] J. Jonkman, S. Butterfield, P. Passon, T. Larsen, T. Camp, J. Nichols, J. Azcona, and A. Martinez, “Offshore Code Comparison Collaboration within IEA Wind Annex XXIII : Phase II Results Regarding Monopile Foundation Modeling,” in *IEA European Offshore Wind Conference*, 2008.

[18] M. Banic, D. Stamenkovic, V. Miltenovic, M. Milosevic, A. Miltenovic, P. Djekic, and M. Rackov, “Prediction of heat generation in rubber or rubber-metal springs,” *Therm. Sci.*, vol. 16, no. suppl. 2, pp. 527–539, 2012.

[19] V. Giavotto, M. Borri, P. Mantegazza, and G. Ghiringhelli, “Anisotropic beam theory and applications,” *Comput. Struct.*, vol. 16, pp. 403–413, 1983.

[20] J. P. Blasques and R. D. Bitsche, “BECAS - an Open-Source Cross Section Analysis Tool Motivation & Overview,” presented at DTU Wind Energy, 2012.

[21] P. Blasques, “User’s Manual for BECAS A cross section analysis tool for anisotropic and inhomogeneous beam sections of arbitrary geometry,” Roskilde, Technical University of Denmark, 2012.

[22] P. Blasques, R. Bitsche, V. Fedorov, and M. Eder, “Applications of the BEam Cross section Analysis Software (BECAS),” proceedings of the 26th Nordic Seminar in Computational Mechanics, Department of Wind Enery, Technical University of Denmark, Roskilde, 2013.

[23] R. D. Bitsche, “Airfoil2BECAS : A preprocessor for the cross-section analysis software BECAS,” Technical University of Denmark, 2012.

[24] C. Sequeira, D. Willis, and J. Peraire, “Comparing Aerodynamic Models for Numerical Simulation of Dynamics and Control of Aircraft,” *44th AIAA Aerosp. Sci. Meet. Exhib. Massachusetts Inst. Technol.*, 2006.

[25] T. J. Larsen and A. M. Hansen, *How 2 HAWC2 , the user ’ s manual*. Technical University of Denmark, Roskilde, 2013.

[26] A. Labuschagne, N. F. J. van Rensburg, and a. J. van der Merwe, “Comparison of linear beam theories,” *Math. Comput. Model.*, vol. 49, no. 1–2, pp. 20–30, 2009.

[27] A. Yde, D. Verelst, and T. J. Larsen, “Structural Model; E-lesson 1: Introduction to Flexible Multibody Dynammics,” Technical University of Denmark, Roskilde, 2013.

[28] A. Yde and T. J. Larsen, “HAWC2-an introduction. A Servo-Aeroelastic Wind Turbine Simulation Tool. Online Lecture,” Technical University of Denmark, Roskilde, 2013.

[29] A. Yde, D. Verelst, and T. J. Larsen, “Aerodynamic Model; E-lesson 2: Rotor Aerodynamics,” Technical University of Denmark, Roskilde, 2013.

[30] F. Rasmussen, J. T. Petersen, P. Vølund, P. Leconte, E. Szechenyi, and C. Westergaard, “Soft rotor design for flexible turbines,” Technical University of Denmark, Roskilde, 1998.

[31] N. Timmer, “Introduction to Wind Energy; Energy production,” Delft University of Technology, 2013.

[32] W. Bierbooms, “Offshore Wind Climate,” Delft University of Technology, 2013.

[33] V. Fedorov, N. Dimitrov, C. Berggreen, S. Krenk, K. Braner, and P. Berring, “Investigation of Structural Behavior due to Bend-Twist Couplings in Wind Turbine Blades,” Technical University of Denmark, Roskilde, 2010.

[34] L. Mishnaevsky, “Composite materials in wind energy technology,” in *Thermal to mechanical energy conversion: engines and requirements*, Technical University of Denmark, Roskilde, 2011.

[35] I. De Baere and J. Degrieck, “Composites, Macroscopic behaviour of one ply,” University of Ghent, 2013.

[36] P. A. Lagace, “Static tensile fracture of graphite/epoxy,” Massachusetts Intitute of Technology, 1982.

[37] R. Koide, G. França, and M. Luersen, “An ant colony algorithm applied to lay-up optimization of laminated composite plates,” *Lat. Am. J. Solids …*, vol. 10, pp. 491–504, 2013.

[38] L. S. BV, “Kolibri - Composite conceptual design and analysis tool.” [Online]. Available: http://www.lightweight-structures.com/kolibri-composite-conceptual-design-and-analysis-tool/index.html. [Accessed: 28-Jun-2015].

[39] D. G. Lee and N. P. Suh, *Axiomatic Design and Fabrication of Composite Structures - Applications in Robots, Machine Tools, and Automobiles*. Oxford University Press, 2006.

[40] E. Hau, *Wind Turbines: Fundamentals, Technologies, Application, Economics*, 2nd ed. Springer Berlin Heidelberg, 2006.

[41] D. Lobitz and P. Veers, “Aeroelastic behavior of twist-coupled HAWT blades,” ASME Wind Energy Symposium, American Institute of Aeronautics and Astronautics, 1998.

[42] L. Fingersh, M. Hand, and A. Laxson, “Wind Turbine Design Cost and Scaling Model,” National Renewable Energy Laboratory, USA, 2006.

Appendix A Aeroelastic instabilities related to bend-twist coupling

This section addresses the main aeroelastic instabilities and the effect of an increased bend-twist to feather coupling on these instabilities which is shortly explained in section 2.4.

In general the three main aeroelastic instabilities which may arise are [40]:

- **Static divergence:** This effect depends on the relative position of the elastic axis and the aerodynamic centre. The aerodynamic centre, which is the attachment point of the lift forces, mostly lies around the quarter chord length. The elastic axis location depends on the structural build-up of the blade. If this is located behind the aerodynamic centre, the lift creates a nose-up moment around the airfoil which increases the angle of attack relative to the square of the free-stream velocity. The restoring moment from the wings torsional stiffness is independent of the speed so at a certain speed, the so called divergence speed, a torsional instability develops and the blade collapses.
- **Classical flutter:** This is a two degree of freedom oscillation: a combined pitch and plunge movement of the blade. The effect occurs in general when the pitch and plunge motion over one cycle are so that the lift on average aligns with the motion rather than opposing it.
- **Stall flutter**: Especially for a stall controlled wind turbine this effect may be crucial. A one degree of freedom periodic change in pitch between flow separation and normal flow may occur close to the angle of attack at which the blade goes in stall. The large induced vibrations may be in flapwise or in edgewise direction.

If wind turbine blades are made more flexible or the bend-twist coupling is increased significantly, the stability will become a critical design issue. More torsional flexibility in the blades combined with the wing sweep will induce a higher bend-twist coupling effect. As described in [41] NASTRAN is used to calculate instabilities with respect to the amount of coupling. A negative “fraction of available coupling” is relevant for this research since the wing is swept backwards inducing the twist to-feather coupling. The two instabilities, divergence and classical flutter, behave oppositely. The blade is more stable regarding divergence by increasing the amount of coupling. The classical flutter speed is an issue however. As can be seen in Figure 42 the critical flutter speed reduces due to a gain in twist-to-feather coupling. The flutter speed is the limiting stability issue if the twist-to-feather coupling is increased. As [9] describes also stall flutter is not increased when significant twist to feather couplings are applied.

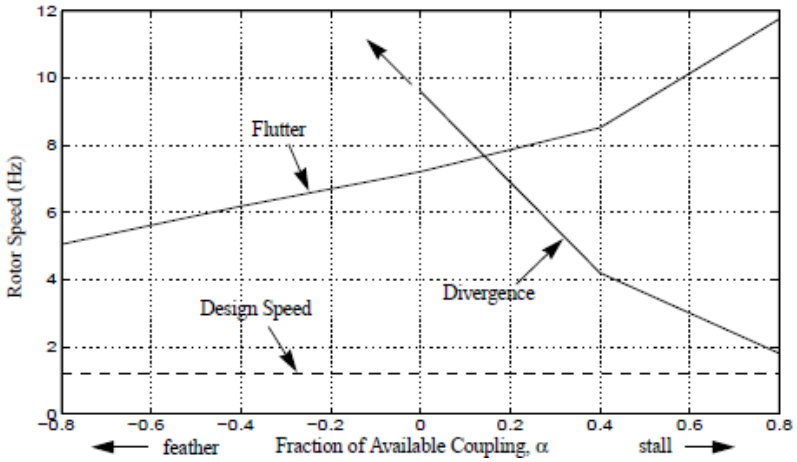

Figure 42 – Aeroelastic stability boundaries for a bend-twist coupled blade. This research focusses on increasing the twist-to-feather coupling of the blade. The figure shows that in this case the flutter behaviour gets more critical while divergence limits increase. [41]

Appendix B Section reduction

This section describes the section reduction which is related to the generation of the structural file with BECAS as described in section 3.5.3. Currently the blade structural file of the HAWC2 model of the XANT M-21 consists of 28 structural sets spread over the blade. Preparing and simulating a cross section in BECAS takes a considerable amount of time, therefore the amount of sections is further reduced. To see how many sections can be used dynamic HAWC2 simulations are performed over the operating wind speed range with 28, 11 and 6 cross sections. As can be seen in Figure 43 the simulation results using 6 structural sets are different from the simulation results when 28 structural sets are used. Therefore it is concluded that 6 sections is too few to correctly model the blade.

Figure 43 shows that when 11 cross sections are used the flapwise displacements, root bending moment, power and thrust are negligibly different. This means that 11 sections, one section every meter, is enough to model the whole blade instead of using 28 sections.

Near the root many sections have to be modelled to capture the fast changing layup scheme. To capture the blade root mass and stiffness in more detail the amount of sections near the root is increased. Finally 14 sections are used to model the blade.

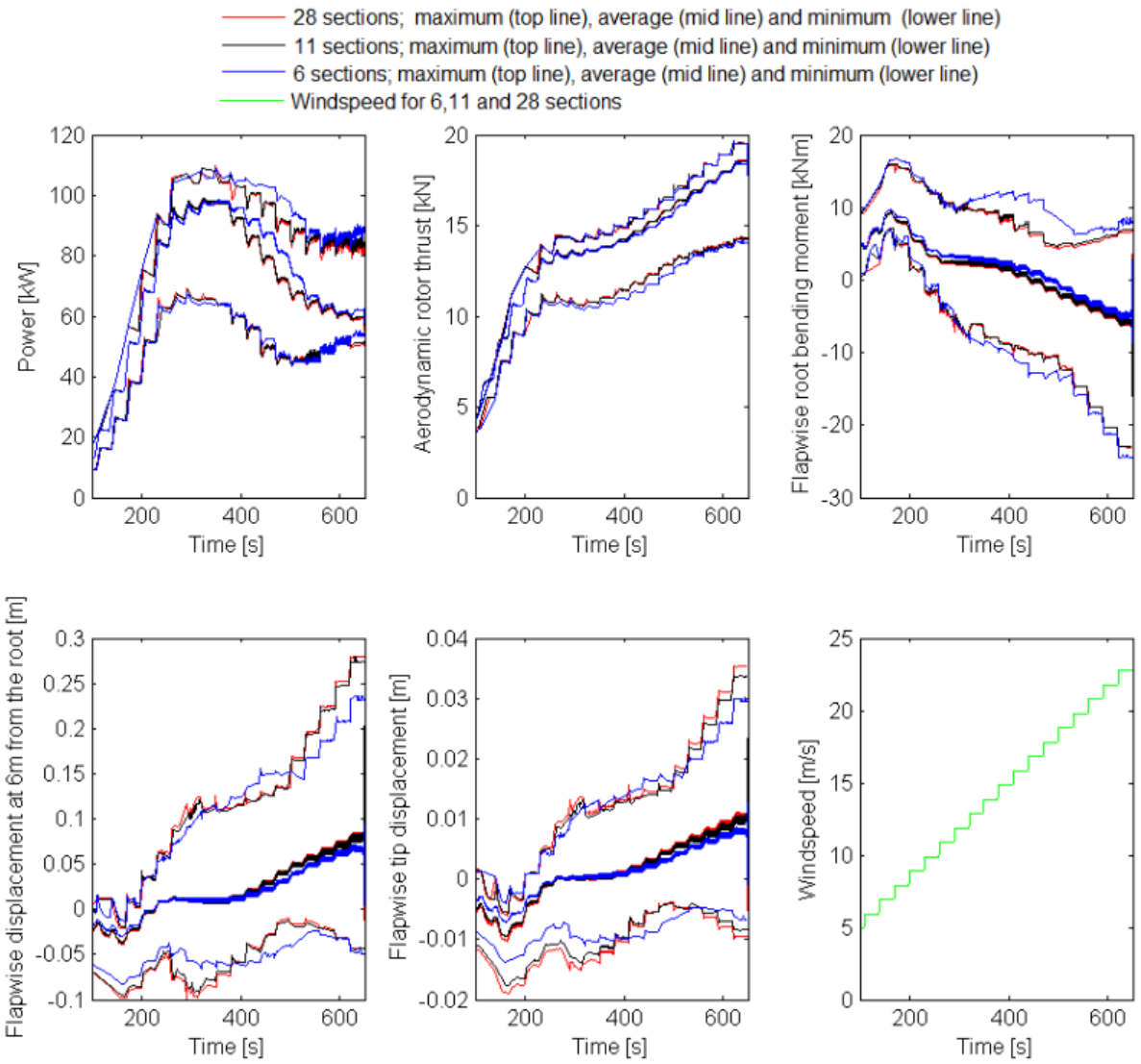

Figure 43 - HAWC2 dynamic simulation in the operational wind speed range, simulation results of which the blade is composed of 6, 11 or 28 structural sections

Appendix C Nonlinear modelling

As indicated in the recommendations in Chapter 7 modelling with nonlinear material stiffness might be required to correctly model highly flexible wind turbine blades. The original plan was to include these material nonlinearities in the simulation. A nonlinear simulation setup is designed using HAWC2 and BECAS of which an overview can be seen in Figure 44. The stress-strain-recovery function of BECAS can be used to calculate all local stresses and strains of every finite element of every cross section. By updating the stiffness values for every location in BECAS a new simulation can be performed. By making this process converge the final loading and displacements including the nonlinear material characteristics can be found.

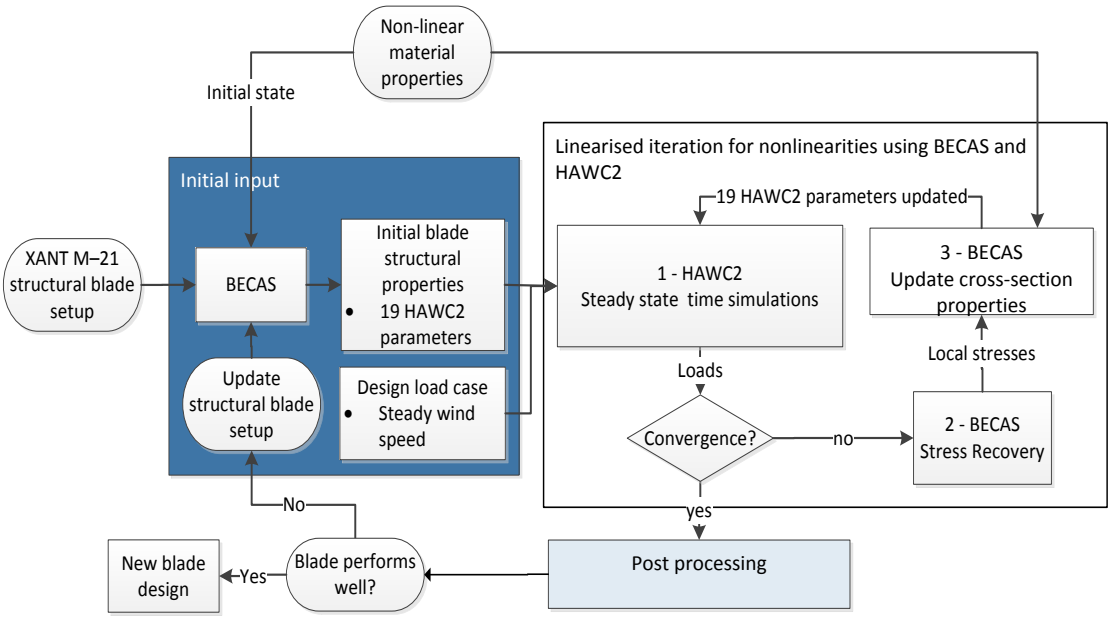

Figure 44 – Modelling of nonlinear materials in wind turbine blades with BECAS and HAWC2: a setup

However several challenges arise when including material nonlinearities:

- **Extra iteration loop:** When the loads are calculated with linear materials, the stiffness is used to find the corresponding displacement. When material nonlinearities are included the stiffness itself needs to be calculated in an extra iteration loop. This increases the complexity of the model, slows down the calculation time and induces an extra convergence criterion.
- **Steady state dynamic simulations**: In this iteration loop the stiffness should be iterated for every new load case. In the case of HAWC2 it is currently not possible to change or even pause the time sequence of the simulations. A solution would be to perform steady state simulations. Steady state means constant loading and therefore no wind shear, no tower

shadow and no gravity. HAWC2 should be restarted for every steady-state simulation. This would increase the simulation time and make it impossible to include dynamic simulations.

- **Stiffness update challenges**: The stiffness properties used in HAWC2 simulations should be updated based on the loading. The BECAS stress recovery function can be used to find the stress of every element of every cross section in every direction under a certain loading. From these stress distributions the new stiffness parameters can be defined and updated. Unfortunately the stiffness value gained from this nonlinear stiffness method is not correct: an example of a stress-strain curve of a nonlinear element is shown in Figure 45. As can be seen a local stress s1 will give a stiffness E_1. However since HAWC2 works with linear stress strain characteristics, the real stiffness seen by HAWC2 corresponds to E_{1_HAWC2} in Figure 45. The strain which is calculated by HAWC2 (r_{1_HAWC2}) is larger than it should be (r_1).

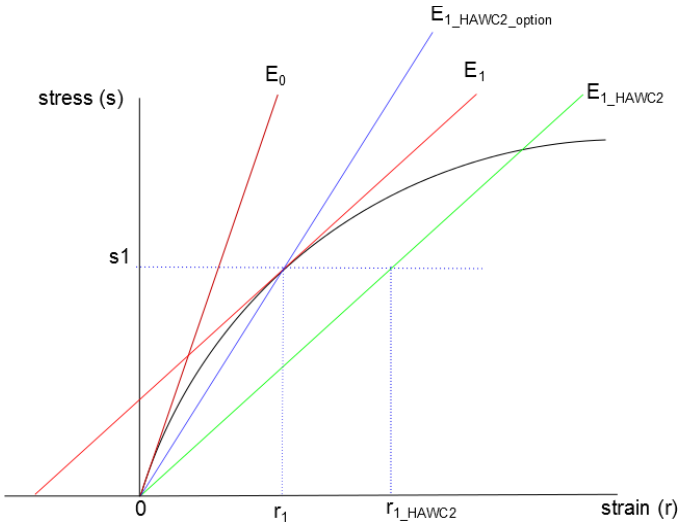

Figure 45 – Material stiffness update.

Options proposed to deal with the stiffness update challenges:

- Introduce an **offset in the stress strain curve in HAWC2**, use E1 in Figure 45 directly in HAW2. This would involve a change in the source code of HAWC2 which is technically very complicated and furthermore HAWC2 is not an open source software. Using another aeroelastic solver could be another option.
- Use an **alternative stiffness** $E_{1\_HAWC2\_option}$ which corresponds to the blue line in Figure 45. This stiffness only gives the correct deformations if it has converged completely. Once the stress values are a little off it will give strain values which are not on the stress-strain curve anymore. This is not the most "beautiful" option but might be able to make the current methodology plausible.

- Implement a **nonlinear beam element** or connect it to an open source nonlinear beam model and connect it to HAWC2 using the external systems DLL interface. This will be very difficult and it is not clear yet if this will be even possible with HAWC2.

Modelling nonlinear material properties with an aeroelastic design tool is not convenient. This is a major challenge to overcome when highly nonlinear materials are used.

Appendix D HAWC2 twist output

The twist of the blade is an important parameter when designing flexible blades since flexibility in twist direction gives the best results as is shown in Chapter 5. In HAWC2 four different blade twist outputs are available which all show a different twist angle. The twist in the blade root coordinate system is required which is not one of them. The *aero rotation* command is close, but cannot cope with a swept blade planform near the tip.

To model the twist over the blade, massless dummy bodies are created and connected to the blade at different lengthwise locations. By comparing the displacements at the ends of these dummy bodies, the local change in blade twist angle is calculated with the basic goniometric equation 6 where Δx is the in-plane displacement tangential to the rotation, Δy is the out of plane displacement and Δz is the radial in-plane displacement. The displacements are with respect to the reference frame of the root of the blade.

$$\theta_{twist} = \theta_{initial\ twist} + atan\left(\frac{\Delta y}{\sqrt{(\Delta x)^2 + (\Delta z)^2}}\right) \tag{6}$$

The difference between the *aero rotation* outputs and the results using the dummy files is shown in Figure 46 which presents twist deformations over the blade at a sudden wind speed of 70m/s in parked condition. As can be seen the resulting rotations are nearly the same up to 6m from the root. There is a small difference in radial position which causes the small offset up to 6m from the root. For the swept part of the blade, which starts at 6 m from the root up to the tip of the blade, the dummy-based twist angle shows the expected behaviour while the aero rotation output goes to an illogical value which shows it does not take into account the sweep of the blade correctly.

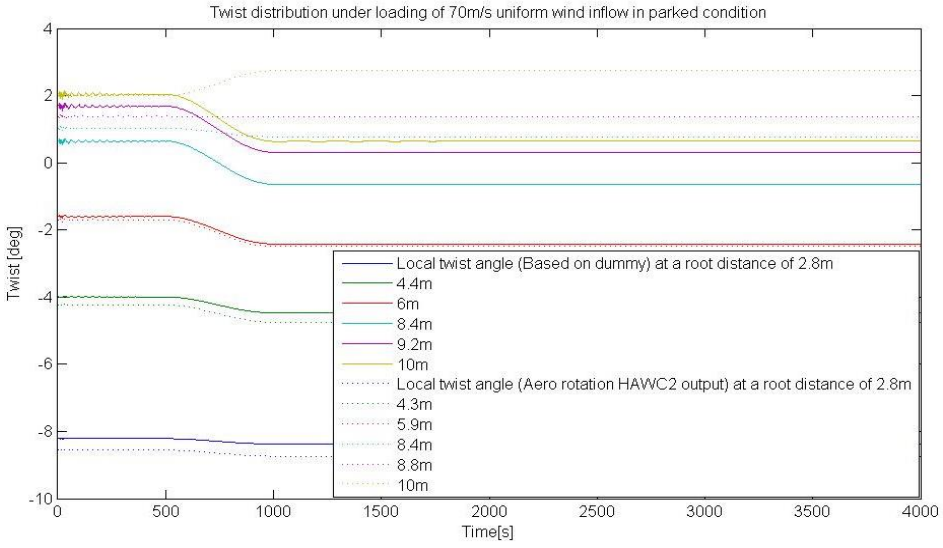

Figure 46 – Calculation of the blade twist: automatic HAWC2 method versus manual dummy method

Appendix E Load reduction to cost relation

The load reduction to cost relation is one of the recommendation for further research in Chapter 7. By reducing the peak loads many components of the wind turbine such as the blade hub, tower, foundation, etc. can be downsized and therefore the wind turbine can be made cheaper. Some main scaling rules have been developed as described by [42] but these are only available for larger wind turbines (> 2MW) and cannot be used for the current 100 kW wind turbine. Also there are some parts of the wind turbine which already have a minimum dimension (tower wall thickness, casted hub thickness) which cannot be downscaled easily. Therefore a good direct relation between the maximum loads and the cost-of-energy is very difficult to obtain. Another way of translating this load reduction to cost is by increasing the blade length and therefore increasing the loads up to the original level. The energy yield of this longer blade will be increased while maintaining the same blade hub, tower, foundation, etc. Therefore the cost of the wind turbine can be assumed to remain the same while the energy yield increases which results in a reduction in cost of energy.

Appendix F Manual master thesis software tool

To make the current research usable for future research a manual is made. This manual describes the steps to perform simulations with the tool developed for this thesis work as well as the required software tools to perform these simulations. This manual corresponds to the modelling data and software tools "FlexMod_Example_1.0".

F.1 Required software

Some software tools are required to use the modelling tool. The main software tools are:

- HAWC2 version 11.5
- MATLAB version R2012b
- BECAS version 2.3

To perform simulations with BECAS extra supporting software tools are required:

- Python version 3.3, 64 bit
- Numpy 64 bit version
- SciPy

F.2 User's manual

This user's manual describes step by step to design new blades made of new materials and analyse the behaviour.

F.2.1 Adapt the input Matrix

1. Open/create the input matrix MatProps1.xlsx, MatProps2.xlsx or … in folder ..\Organize_input\MatProps1.
2. Give a name to the new load case on **location A** in Figure 47
3. Give/change the material properties on **location B** in Figure 47. Different material types have been identified in the blade of which the material properties can be changed separately:
    - M1_PVC: the foam in the shear web
    - M2_BIAX: the biaxial composite material layers in the blade, except for the axial material in the shear web
    - M3_BIAX_shear: the biaxial composite material in the shear webs
    - M4_UNIAX_sparcap: the uniaxial composite material located in the sparcaps
    - M5_UNIAX_root: the uniaxial composite material located in the blade (only present in the root section)
    - M6_Balsa: balsa wood used in the blade skin
    - M7_CFM: layer located in the blade skin to improve the resin transmission in the spar cap
4. The material behaves as a homogeneous ply. The homogeneous ply properties of every material type can be seen at **location C in** Figure 47. These are the parameters which can be changed manually for every material type:

- The Young's modulus in three directions
- The Poisson coefficient in three directions
- The shear modulus in three directions
- The density of the ply
- The thickness of the ply

5. Save every new structural blade set as a new MatProps file (MatProps1.xlsx, MatProps2.xlsx, …)

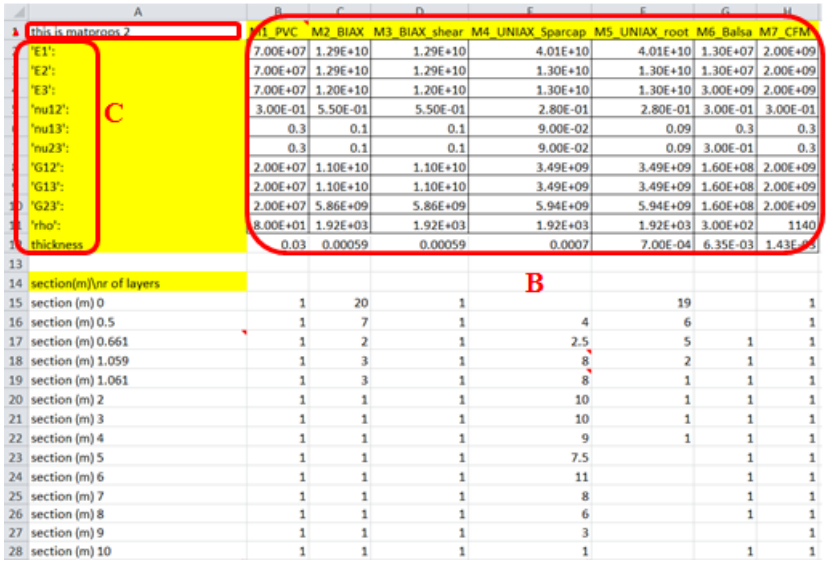

	A	B	C	D	E	F	G	H
1	this is matprops 2	M1_PVC	M2_BIAX	M3_BIAX_shear	M4_UNIAX_Sparcap	M5_UNIAX_root	M6_Balsa	M7_CFM
2	'E1':	7.00E+07	1.29E+10	1.29E+10	4.01E+10	4.01E+10	1.30E+07	2.00E+09
3	'E2':	7.00E+07	1.29E+10	1.29E+10	1.30E+10	1.30E+10	1.30E+07	2.00E+09
4	'E3':	7.00E+07	1.20E+10	1.20E+10	1.30E+10	1.30E+10	3.00E+09	2.00E+09
5	'nu12':	3.00E-01	5.50E-01	5.50E-01	2.80E-01	2.80E-01	3.00E-01	3.00E-01
6	'nu13':	0.3	0.1	0.1	9.00E-02	0.09	0.3	0.3
7	'nu23':	0.3	0.1	0.1	9.00E-02	0.09	3.00E-01	0.3
8	'G12':	2.00E+07	1.10E+10	1.10E+10	3.49E+09	3.49E+09	1.60E+08	2.00E+09
9	'G13':	2.00E+07	1.10E+10	1.10E+10	3.49E+09	3.49E+09	1.60E+08	2.00E+09
10	'G23':	2.00E+07	5.86E+09	5.86E+09	5.94E+09	5.94E+09	1.60E+08	2.00E+09
11	'rho':	8.00E+01	1.92E+03	1.92E+03	1.92E+03	1.92E+03	3.00E+02	1140
12	thickness	0.03	0.00059	0.00059	0.0007	7.00E-04	6.35E-03	1.43E-0
13								
14	section(m)\nr of layers							
15	section (m) 0	1	20	1		19		1
16	section (m) 0.5	1	7	1	4	6		1
17	section (m) 0.661	1	2	1	2.5	5	1	1
18	section (m) 1.059	1	3	1	8	2	1	1
19	section (m) 1.061	1	3	1	8	1	1	1
20	section (m) 2	1	1	1	10	1	1	1
21	section (m) 3	1	1	1	10	1	1	1
22	section (m) 4	1	1	1	9	1	1	1
23	section (m) 5	1	1	1	7.5		1	1
24	section (m) 6	1	1	1	11		1	1
25	section (m) 7	1	1	1	8		1	1
26	section (m) 8	1	1	1	6		1	1
27	section (m) 9	1	1	1	3			1
28	section (m) 10	1	1	1	1		1	1

Figure 47 – MatProps input matrix

F.2.2 Prepare and perform the pre-processing

BECAS

6. Open Tweak_text_file_v1.m in the folder BECAS_input.
7. Change the variable BECASLocation to the current location of the BECAS file runBECAS.m, the main matlab file which starts all sub-models of BECAS. This is located in the main folder of BECAS.
8. Open Generate_htc_file_end.m in the folder htc_generation_txt_files.
9. Change the variable HAWC2_model_name to the current name of the "HAWC2-model" in the main folder (e.g. HAWC2_Model_RBR5b_SRE6c)
10. Open Generation_HAWC2_file.m in the main folder
11. Change "cases_to_analyse" to the input matrices you want to simulate (see section F.1)
12. Run Generation_HAWC2_file.m

Combination

13. Open ST1.txt, ST2.txt and ST3.txt,… in the folder "Combination" and past structural file properties from structural_file.st in the folder HAWC2_Model_Name\data.
14. Open Combination/CombinationOverview.xlsx and fill in 1, 2, 3, 4 or 5 for every section which indicates if the properties of ST1.txt, ST2.txt, ST3.txt, ST4.txt or ST5.txt are taken respectively (see Figure 48).

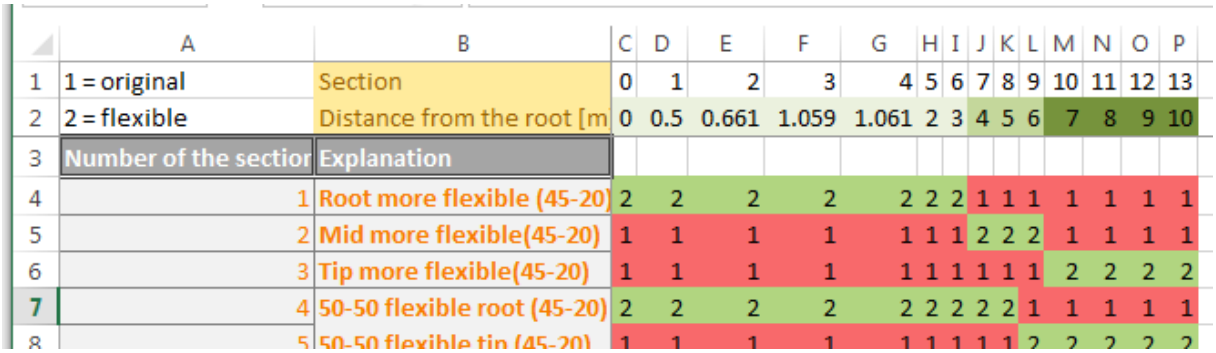

	A	B	C	D	E	F	G	H	I	J	K	L	M	N	O	P
1	1 = original	Section	0	1	2	3	4	5	6	7	8	9	10	11	12	13
2	2 = flexible	Distance from the root [m	0	0.5	0.661	1.059	1.061	2	3	4	5	6	7	8	9	10
3	Number of the sectior	Explanation														
4	1	Root more flexible (45-20)	2	2	2	2	2	2	2	1	1	1	1	1	1	1
5	2	Mid more flexible(45-20)	1	1	1	1	1	1	1	2	2	2	1	1	1	1
6	3	Tip more flexible(45-20)	1	1	1	1	1	1	1	1	1	1	2	2	2	2
7	4	50-50 flexible root (45-20)	2	2	2	2	2	2	2	2	2	1	1	1	1	1
8	5	50-50 flexible tip (45-20)	1	1	1	1	1	1	1	1	1	2	2	2	2	2

Figure 48 - CombinationOverview.xlsx

15. Open and run Combination/Combination2.m
16. Copy Combination/structural_file_combo.st to HAWC2_Model_RBR5b_SRE6c\data\structural_file.st under the other cases.

F.2.3 Prepare and perform the processing

17. Open the HAWC2 multimodel Multimodel.xlsm in the HAWC2 folder HAWC2_Model_Name.
18. Three load cases are considered which can be seen on location A in Figure 49. Every load case has several rows with a different blade structural set number (see location C in Figure 49). Make sure there are at least as many rows for every load case than there are MatProps files in the folder Organize_input\MatProps1. Add more rows for all three load cases if needed. Make sure the structural blade set number of location C continuously increases as in the example.
19. Indicate on location B in Figure 49 which cases should be analysed by writing a number. Make sure that if e.g. case three is selected, the case three in the all three load cases is selected.
20. Change the name of the HAWC2 multimodel if needed in location A in Figure 50.
21. Press on the  -icon (location D in Figure 49)
22. Perform the simulations

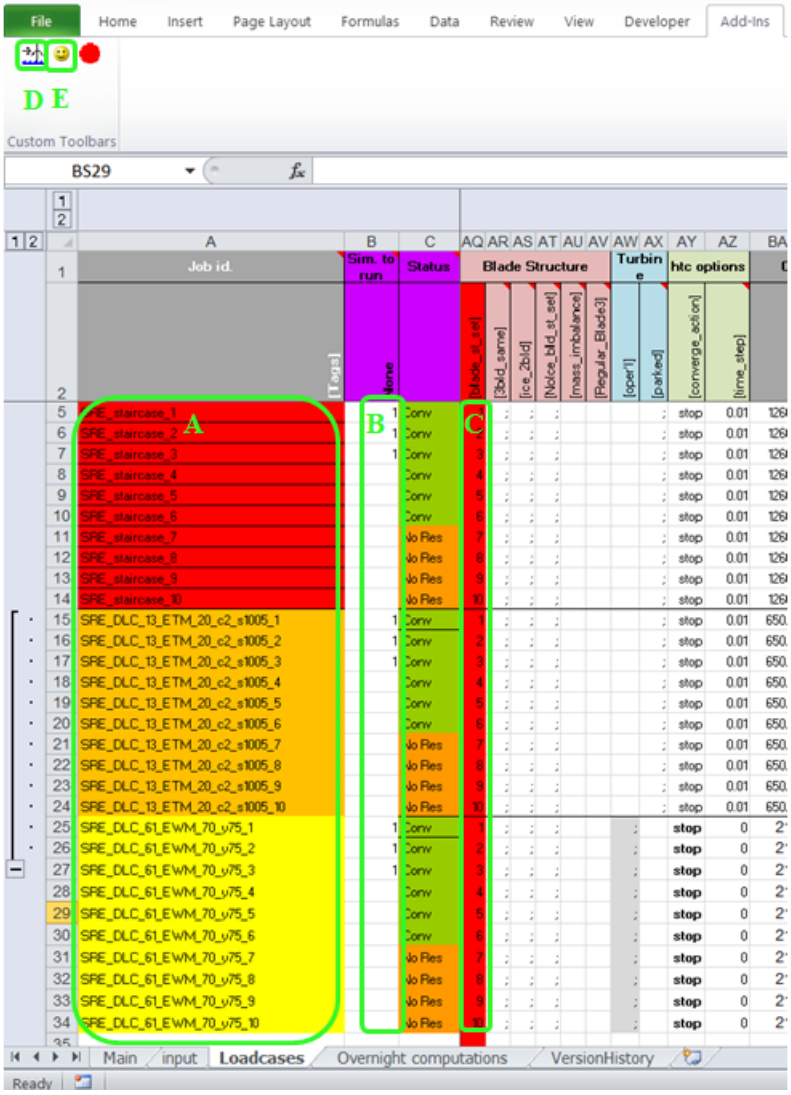

Figure 49 – Excel Multimodel 1

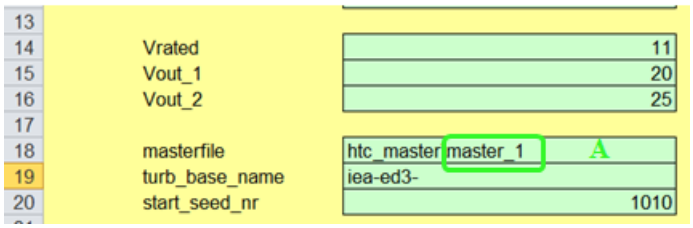

Figure 50 – Excel Multimodel 2

F.2.4 Prepare and perform the post-processing

23. Press on the 🙂-icon (location E in Figure 49)
24. Save and close the HAWC2 multimodel.
25. Open Postprocessing10.m in folder HAWC2_Model_Name\iec_res

26. Change the variable “number of cases” to the total amount of cases present in the Excel Multimodel (in the case of Figure 49 this would be 10).
27. Change the variable “number of cases considered” to the total amount of cases considered (in the case of Figure 49 this would be 3)
28. Change the variable “multimodel” to the name of the current multimodel. In this example case this is “Multimodel.xlsm”.
29. Run Postprocessing10.m
30. Open the Multimodel.xlsm in the HAWC2 folder HAWC2_Model_Name. The final maximum thrust, annual energy yield and cost-of-energy can be seen on the right side of sheet “load cases”.
31. The explanations corresponding to these results can be found in
    a. IM_description.xlsx located in the main folder
    b. CombinationOverview.xlsx located in the folder “Combination”